Impact of Hydrogen Pick-Up and Applied Stress on C-Component Loops: Toward a Better Understanding of the Radiation Induced Growth of Recrystallized Zirconium Alloys

L. Tournadre, F. Onimus, J.-L. Béchade, D. Gilbon, J.-M. Cloué, J.-P. Mardon, X. Feaugas

Impact of hydrogen pick-up and applied stress on c-component loops: toward a better understanding of the radiation induced growth of recrystallized zirconium alloys

L. Tournadre[1], F. Onimus[1]*, J.-L. Béchade[1], D. Gilbon[1], J.-M. Cloué[2], J.-P. Mardon[2], X. Feaugas[3]

[1]CEA, DEN, Service de Recherches Métallurgiques Appliquées (SRMA) 91191 Gif-Sur-Yvette, France
[2]AREVA AREVA NP Fuel BusinessUnit10, Rue Juliette Recamier 69456, Lyon Cedex, France
[3]LaSIE, FRE CNRS 3474, Université de La Rochelle, 17042 La Rochelle Cedex 1, France
*corresponding author: fabien.onimus@cea.fr

Under neutron irradiation, recrystallized zirconium alloys, used as structural materials for Pressurized Water Reactor (PWR) fuel assemblies, undergo stress-free growth which accelerates for high irradiation doses. This acceleration is correlated to the formation of c-component vacancy dislocation loops lying in the basal plane. The growth behavior observed on some PWR fuel assemblies suggests that a macroscopic stress applied under irradiation could affect the c-loop microstructure and therefore influence the subsequent stress-free growth. In addition, some feedbacks show that in-service hydrogen pick-up could also influence the fuel assembly radiation-induced deformation.

The impact of an applied stress on c-loops has been studied on as-received recrystallized Zircaloy-4 (RXA Zy-4) irradiated with 300 keV and 600 keV Zr ions at 573 K. An original device, specifically designed for the irradiation facility, apply a stress which relaxes during the early stage of irradiation. In these conditions, observations by Transmission Electron Microscopy (TEM) reveal no effect of the initial applied stress on c-loops. However, when the stress is applied when c-loops are already created, c-loop growth is affected.

Moreover, 2 MeV proton irradiations performed on as-received and pre-hydrided M5[TM][1] and RXA Zircaloy-4 materials were conducted at 623 K. For both grades, the c-component loop evolution with dose is examined and compared to neutron irradiated microstructures. As for neutron irradiated materials, the c-loop density in Zircaloy-4 is higher than in M5[TM]. For pre-hydrided RXA Zircaloy-4 the effect of hydrogen is not significant since the loops are already present in high density. On the other hand, TEM observations on pre-hydrided M5[TM] highlight that c-loop density is higher, far from hydrides, than without pre-hydriding. Furthermore, a high c-loop density is observed in the surrounding of hydrides partially or fully dissolved. To explain these observations the role played by hydrogen in solid solution and as precipitated hydrides is discussed.

---

[1] M5[TM] is a trademark of AREVA NP registered in the USA and in other countries

1. Introduction

Zirconium alloys are used as cladding and structural material for Pressurized Water Reactor (PWR) fuel assemblies. During in-reactor normal operation, the length of the PWR fuel assembly evolves under irradiation. This dimensional change is the result of three main different phenomena: the thermal creep, the irradiation creep and the stress free growth [1-3]. The stress-free growth phenomenon corresponds to an elongation along the basal plane of the hexagonal close packed structure and a shortening along the c-axis, the volume remaining constant [4]. Due to the marked texture of zirconium tubes [5], the growth of the hexagonal close packed grains, at the microscopic scale, leads to a macroscopic elongation along the axial direction of the tubes. For recrystallized zirconium alloys, at high fluence, typically after an incubation dose of 4.0×10^{25} n.m^{-2} (corresponding to 6 dpa, E>1 MeV) [6], the growth rate increases. This acceleration is often referred to as "breakaway growth". Some feedbacks from industry [7, 8] show that external parameters like an applied stress or in-service hydrogen pick-up could also increase the resultant deformation after the "breakaway growth". Since the growth acceleration can have a significant impact on the performance of the fuel assembly this phenomenon has to be well understood and predicted.

According to several authors, the breakaway growth is clearly correlated to the nucleation at high doses of a specific microstructural irradiation defect: the c-component dislocation loops [9]. C-component loops have already been observed after neutron irradiations [10, 11], but also after charged particle irradiations conducted with electrons [12-14], heavy ions [15-17] and protons [15]. C-loops are of vacancy type only and are located in the basal plane. When they are observed after neutron irradiation by Transmission Electron Microscopy (TEM), they are faulted and their Burgers vector, given by $\underline{b} = 1/6 < 20\bar{2}3 >$, has a component along the c-axis [11]. Whatever the irradiation conditions, these c-component loops, which appear after an incubation dose, are always present in conjunction with more numerous and finer a-loops which appear from low irradiation dose. The c-component loops are much larger than the a-loops but their number density is much lower. For instance, for recrystallized Zircaloy-2 and Zircaloy-4 irradiated at 573 K, after 5.4×10^{25} n/m^2, c-component loops are found with a diameter of 120 nm and with a number density between 3 and 6×10^{20} m^{-3} whereas the a-loops density saturates at a value of 3×10^{22} m^{-3}, from a relatively low fluence of approximately 2×10^{24} n/m^2 [3] with a diameter of about 7 nm. Due to the high density of small a-loops, the c-component loops can only be observed edge-on by TEM by using the $\underline{g}$=0002 diffraction vector, which leads to invisible a-type defects. The c-loops thus appear as straight-line segments.

It is rather surprising that although the most stable loops in zirconium alloys are the prismatic loops, in agreement with the Foll and Wilkens criterion ($c/a < \sqrt{3}$) [18], basal loops are also observed. Moreover, these loops are of the vacancy character. According to the usual rate theory, vacancy loops should not grow as a result of the bias of edge dislocation toward self-interstitial atoms (SIA). The reason for the nucleation and growth of c-component loops in zirconium alloys has been analyzed and discussed in great detail by Griffiths and co-workers [11, 19, 20] but this phenomenon is still not well understood. It has been shown by Molecular Dynamics computations for α-zirconium [21] that most of the small interstitial clusters produced in the displacement cascade have the form of a dislocation loop with Burgers vector <a> = $1/3 < 11\bar{2}0 >$. Small vacancy clusters are also found in the prismatic plane. On the other hand, vacancy clusters in the basal plane form a hexagonal loop enclosing an extrinsic (E) stacking fault with ½<0001> Burgers vector. As reviewed by Hull and Bacon [22], condensation of vacancies in a single basal plane results in two similar atomic layers coming into contact. This unstable situation of high energy is avoided in one of two ways described by Berghezan et al. [23] implying the glide of partial dislocations in the platelet plane. The first process leads to the creation of a sessile Frank partial with ½<0001> Burgers vector surrounding a high energy extrinsic (E) stacking fault disk.

-The second process leads to the creation of a sessile Frank partial $1/6 < 20\bar{2}3 >$ Burgers vector surrounding the type I_1 low energy intrinsic stacking fault. The energy of a faulted perfect edge loop with radius R can expressed as Eq. 1 according to the elastic theory [24]. A more comprehensive treatment accounting for the character of the loop can be derived easily.

$$E_{loop}(R) = E_{line} + E_{fault} = 2\pi R \frac{\mu b^2}{4\pi(1-\nu)}\left(ln\left(\frac{4R}{r_0}\right) - 1\right) + \pi R^2 \gamma_{fault} \qquad (1)$$

With μ the shear modulus, ν the Poisson's ratio, b the Burgers vector, r_0 the core radius and γ_{fault} the stacking fault energy.

From this formula, it can be seen that for small loop the energy of the dislocation line dominates but as the loop grow it is the energy of the stacking fault which dominates. As suggested by Hull and Bacon [22], since the E-type c-loop has a higher stacking fault energy than the I_1-type c-loop ($\gamma_E \approx 249 \, mJ/m^2 > \gamma_{I_1} \approx 124 \, mJ/m^2$ [25]) as the loop grows it is likely to transform into the I_1-type c-loop for a critical loop size, in a similar manner to the unfaulting of loops in face-centered cubic metals. The critical loop size for the transformation from E-type loop to I_1-type loop is likely to be influenced by stress or impurity content according to Hull and Bacon [22] since it can affect the stacking fault energy.

There is indeed considerable evidence to show that the formation of c-component loops is dependent on the purity of the zirconium used [11, 14, 20, 26]. This can probably be attributed to the effect of solute elements on the basal stacking-fault energy. It is also possible that small impurity clusters, especially iron in the form of small basal platelets, could act as nucleation sites for these loops [14, 27].

However, according to Griffiths [11], this cannot account alone for the very large vacancy c-component loops observed, since the growth of vacancy loops is not favorable considering the elastic interaction difference between dislocation and SIAs or vacancies. In order to understand the reason for the important growth of the c-component loops, another mechanism must occur. As discussed by Woo [28], the growth of c-component loops is well understood in the frame of the Difference in Anisotropic Diffusion model. Indeed, because of the higher mobility of SIAs in the basal plane rather than along the c-axis (and the quasi-isotropic diffusion of vacancies), dislocations parallel to the c-axis will absorb a net flux of SIAs whereas dislocations in the basal plane will absorb a net flux of vacancies. This can therefore explain why the basal vacancy loops can grow.

The origin of the incubation period before the appearance of c-component loops is not clearly understood. Griffiths et al. [6], explain that the c-loop formation is dependent on the volume of the matrix containing a critical interstitial solute concentration. This volume increases as the interstitial impurity concentration is gradually supplemented by the radiation-induced dissolution of elements such as iron from intermetallic precipitates [14, 19, 29, 30].

According to our current knowledge there is no experimental evidence in the literature showing any effect of the stress on c-loops in zirconium alloys. However there are many papers describing theoretically the effect of stress on loops, especially for Face-Centered Cubic metals despite the scarce experimental evidences, all dating back from the 70's, of this phenomenon [31-33]. Two main mechanisms are described in the literature to explain the effect of an applied external stress on irradiation induced dislocation loops: the Stress Induced Preferential Nucleation (SIPN) mechanism and the Stress Induced Preferential Absorption mechanism (SIPA).

The Stress Induced Preferential Nucleation (SIPN) mechanism is based on the assumption that the stress enhances the loop nucleation depending on the loop orientation with respect to the applied stress [34-36]. The other mechanism is the Stress Induced Preferential Absorption (SIPA) mechanism. According to this mechanism, the stress influences the absorption bias between a point defect and a cluster [37, 38]. Garner et al. [31] have already studied the effect of an applied stress on Frank loops observed after irradiation in austenitic steels. According to these authors, the Frank loop densities are influenced by the deviatoric stress component normal to the loop habit plane. Indeed, these authors

show that depending on their orientation with respect to the applied stress biaxial stress in their case, in some planes the interstitial Frank loop density is higher than in unstressed material and in other planes the loop density is lower than in the unstressed material.

It is known that in-reactor hydrogen pick-up induces elongation of zirconium alloys tubes [39]. However, as it is discussed in [40], due to the very low hydrogen content usually picked up in-service in M5[TM] tubes (around 100 wppm), the amount of growth due to hydrogen can be neglected. In the case of M5[TM] the accelerated irradiation growth is therefore only attributed to c-component loops. To our knowledge there is yet no experimental evidence of any effect of hydrogen on c-loops. Only indirect evidence can be found in the literature concerning the interaction between hydrogen and irradiation defects in zirconium alloys in general. Indeed, several authors [41-43] have shown, by using Differential Scanning Calorimetry (DSC) experiments, that hydrogen solubility limit is higher for neutron irradiated samples than for non-irradiated samples. Moreover, synchrotron X-ray diffraction measurements [44] were performed on neutron irradiated Zircaloy-4 in order to determine the number of precipitated hydrides. A heat treatment at 873 K has been done in order to anneal out the irradiation loops. Diffraction measurements show that the hydrides density increases after post irradiation annealing suggesting that the hydrogen solubility limit decreases when the loops are annealed out. These authors show for instance that at a temperature around 573 K the solubility limit increases from 70 wppm to 180 wppm and at 598 K this solubility limit increases from 100 wppm to 210 wppm due to irradiation. These results imply that hydrogen atoms are trapped on irradiation defects. Especially, for high irradiation doses, the authors [41-43] assume an interaction between hydrogen atoms and c-loops. This is also suggested by high temperature post-irradiation annealing and synchrotron analysis [42] where c- component loops are more stable and remain traps for hydrogen atoms after annealing. Furthermore, Chung et al. [45] have observed the precipitation of micrometric delta-hydrides aligned with c-loops in the basal planes. This observation suggests an interaction between nano-hydrides and c-loops.
As for the influence of stress on c-loops, there is no experimental result in the literature, to our knowledge, that shows an increase of c-loop density with the hydrogen content in the material.

In order to investigate the role of an applied stress and the influence of hydrogen pick-up on c-loops, charged particle irradiations have been performed. Previous studies [15] have shown that 600 keV Zr ion irradiations conducted at 573 K and 2 MeV proton irradiations conducted at 623 K permit to obtain c-loop. Starting from these conditions we have conducted several Zr ion irradiations under an applied stress, using a specific device especially designed for this purpose, on RXA Zy-4 and M5[TM]. Furthermore, 2 MeV proton irradiations have been conducted on pre-hydrided and as-fabricated RXA Zy-4 and M5[TM] samples [46].

In a first part of the paper the materials, used in as-received and pre-hydrided materials conditions, are described. Then the charged particles irradiations and the device to apply a stress on the samples, under irradiation, are detailed. Eventually, the optical microscopy technique and the TEM analysis method are explained with the associated sample preparation. In a second part, the results concerning the influence of an applied stress and the impact of hydrogen are shown. The results are finally discussed in the last part of the paper, considering the nucleation and growth process of point defect clusters in metals under irradiation.

2. Experimental details

2.1   As-received materials

The materials studied are industrial recrystallized zirconium alloys: Zircaloy-4 (Zy-4) and M5[TM]. The chemical composition is given in Table 1. As in previous studies [15, 46], the specimens are taken

from an intermediate product (in the form of thick tube) which exhibits a basal plane transverse texture (Figure 1). The Kearns factors of both tubes are given in Table 2. The final manufacturing stages of TREX include a classical pilgering and recrystallization annealing cycle. The last heat treatment (about two hours at temperatures close to 853 K) produced a recrystallized grain structure with a grain size of 6.2 ± 0.6 µm for RXA Zy-4 and 5.3 ± 0.4 µm for M5^{TM}. The microstructures obtained are rather similar to the microstructures of recrystallized thin tubes. The second phase precipitates are the same as the ones usually found in thin tubes made of M5^{TM} and RXA Zy-4. Chemical analyses of the thick tubes have also shown a very good chemical homogeneity in the thickness of the tube.

Table 1: Chemical composition of recrystallized Zy-4 and M5^{TM} intermediate products (wt%).

Alloy	Sn %	Fe %	Cr %	S %	Nb %	O %
RXA Zy-4	1.35	0.21	0.10	0.0020	-	0.13
M5^{TM}	-	0.0370	-	0.0017	1.0	0.14

Table 2: Kearns factors of recrystallized Zy-4 and M5^{TM} intermediate products

Alloy	f_L	f_T	f_R
RXA Zy-4	0.09	0.53	0.38
M5^{TM}	0.09	0.49	0.42
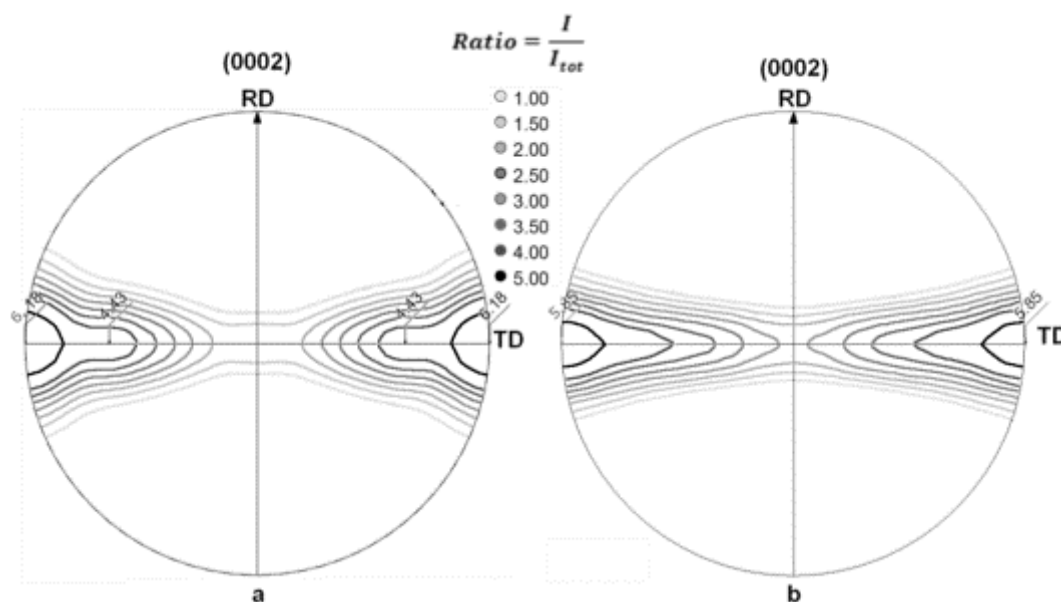
Figure 1 : (0002) pole figures a) RXA Zy-4, b) M5^{TM}

2.2 Pre-hydrided materials

In order to study the effect of hydrogen on c-loops RXA Zy-4 and M5^{TM} samples have been hydrided up to various hydrogen contents. Typical hydrogen contents, representative of in-reactor hydrogen pick-up of 80 wppm for M5^{TM} [47] has been considered here. Furthermore, in order to enhance the potential effect of hydrogen on c-loops, two higher hydrogen contents (125 and 350 wppm) have also been studied. Concerning RXA, Zy-4 the samples have been pre-hydrided up to 185 wppm. Hydriding has been performed under Ar-5%H gas at 673 K in several steps for the highest hydrogen contents.

2.3 Proton irradiations and sample preparation

2 MeV proton irradiations were carried out on the Michigan Ion Beam Laboratory (MIBL / University of Michigan) Tandem accelerator [48] at 623 K under high vacuum up to four different doses. The irradiation temperature of 623 K has been chosen, in agreement with the experiment done by Zu et al. [49], to simulate the in-reactor irradiation temperature of a guide tube which is typically between 573 and 593 K. This temperature shift aims at accounting for the increase in damage rate during proton

irradiation compared to neutron irradiation. The high deposited power per unit surface by the proton beam (4.8×10^5 W/m^2) requires the use of liquid indium at the back of the samples, to extract the deposited heat during irradiation. Furthermore, the temperature is controlled by a 2-dimension thermal camera throughout the experiment in addition to usual thermocouples welded on the samples outside of the beam.

In spite of damage rates higher than for neutrons, several days are required to reach high irradiation doses. The TRIM calculation (Figure 2) shows that the damage peak is obtained between 25 μm and 30 μm depth whereas the damage increases only slowly between 5 μm up to 20 μm depth. The samples are in the form of bars of 20 mm long, 2 mm wide and 1.55 mm thick. The bars are taken in the Axial Direction (AD) – Transverse Direction (TD) plane, the long direction of the bar being along the TD direction. The surface (AD-TD plane) is polished up to a mirror finish before irradiation. After irradiation, the bars are mechanically polished on the back side down to a thickness of 0.1 mm. 3 mm diameter disks are then punched out of the thin strip and usual two-side electro-polishing is performed to remove around 15 μm from the irradiated surface. This surface is then protected with a varnish and the final electro-polishing is performed on the rear surface. Thanks to this specific preparation method, a fully irradiated bulk material is observed by TEM.

All the thin foils were prepared by electro-polishing using a solution of 20% 2-Butoxyethanol and 10 % perchloric acid in ethanol at temperatures around 278 K.

Eight samples can be fully irradiated at the same time during one proton irradiation, and since the irradiated part of the bar is 10 mm long, three thin foils can be taken out of each bar.

It is worth pointing out that, as observed in the previous study [15], the bars after mechanical polishing from the rear surface (100 µm thin strip) systematically exhibit a macroscopic bending which is due to the irradiation induced growth strain of the 30 µm thick irradiated layer, the bending increasing with irradiation dose.

Proton irradiations were performed on as-received RXA Zy-4 and M5^{TM} samples (control samples) and pre-hydrided samples. Irradiation conditions for control samples are given in Table 3. Irradiation conditions for pre-hydrided samples are given with the hydrogen content in Table 4.

During proton irradiations, hydrogen atoms are implanted into the zirconium alloys. Considering the high diffusivity of hydrogen in zirconium at 623 K (diffusion coefficient of 1.2×10^{-10} m^2/s [50]) the hydrogen atoms are probably homogeneously distributed in the whole bar (volume of 62 mm^3). Assuming that there is no desorption, the amount of implanted hydrogen can be estimated for each irradiation dose reached. These values are given in Tables 3 and 4.
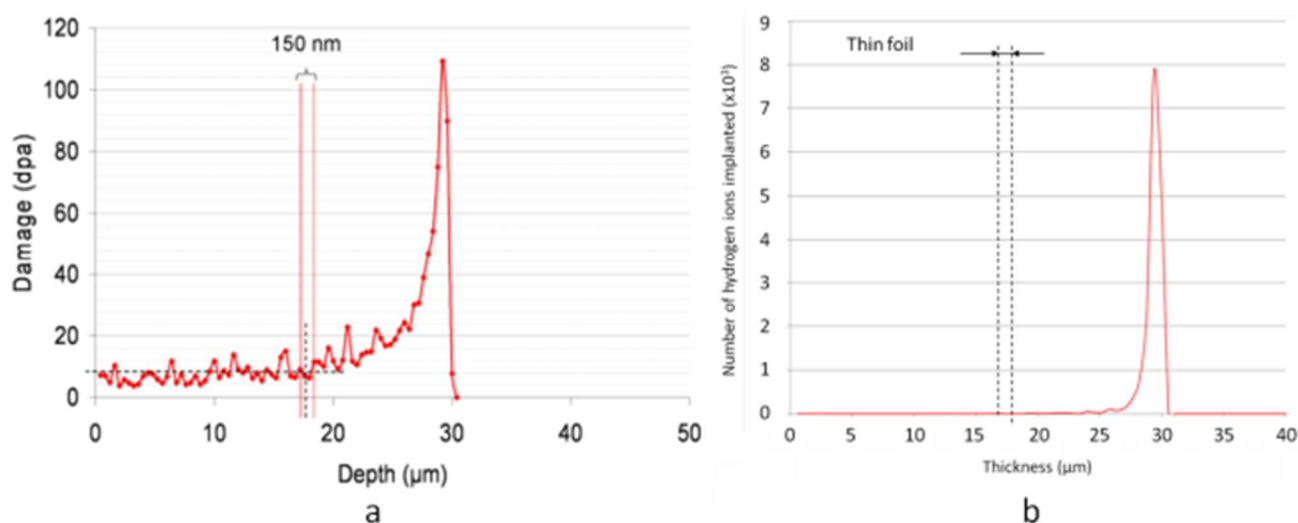
Figure 2 : TRIM calculations for 2 MeV protons in Zr with a dose of $\mathbf{8.9 \times 10^{23}}$ protons/m^2. Zr displacement energy is considered equal to 40 eV. a) Damage profile in dpa; b) implanted hydrogen atoms distribution.

Table 3 : Proton irradiation conditions conducted on as-received M5^{TM} and RXA Zy-4 samples (control samples).

| Material	Dose		T (K)	Damage rate (dpa/s)	Flux (ions/cm²/s)	Duration (h)	Estimated implanted hydrogen wppm
	dpa	ions/cm²					
M5™	4.9	3.50×10^{19}	623	1.50×10^{-5}	1.07×10^{14}	90	29
	8.1	5.78×10^{19}		1.64×10^{-5}	1.17×10^{14}	150	46
	12.5	8.93×10^{19}		2.02×10^{-5}	1.44×10^{14}	200	79
	19	1.36×10^{20}		1.80×10^{-5}	1.28×10^{14}	266	107
Zy-4	8.1	5.78×10^{19}	623	1.64×10^{-5}	1.17×10^{14}	150	46
	12.5	8.93×10^{19}		2.02×10^{-5}	1.44×10^{14}	200	79
	19	1.36×10^{20}		1.80×10^{-5}	1.28×10^{14}	266	107

Table 4 : Proton irradiation conditions conducted on pre-hydrided M5^{TM} and Zy-4 samples.

Material	Dose		Initial hydrogen content (wppm)	Estimated implanted hydrogen wppm	T (K)	Damage rate (dpa/s)	Flux (ions/cm²/s)	Duration (h)
	dpa	ions/cm²						
M5™	4.9	3.50×10^{19}	350	29	623	1.50×10^{-5}	1.07×10^{14}	90
	8.1	5.78×10^{19}	350	46		1.64×10^{-5}	1.17×10^{14}	150
	12.5	8.93×10^{19}	350	79		2.02×10^{-5}	1.44×10^{14}	200
	19	1.36×10^{20}	350	107		1.80×10^{-5}	1.28×10^{14}	266
	19	1.36×10^{20}	80 125 350	107	623	1.9×10^{-5}	1.36×10^{14}	266
Zy-4	19	1.36×10^{20}	185	107	623	1.9×10^{-5}	1.36×10^{14}	266

2.4 Zr ion irradiations and device for applying a stress under irradiation

300 keV and 600 keV Zr ion irradiations were conducted respectively on the IRMA and ARAMIS facilities at CSNSM/IN2P3-Orsay [51-53] at 573 K. At these energies, the heavy ion flux provides a high damage rate in the irradiated layer, and therefore, a high irradiation dose in only one day. The damage profiles created by 300 keV and 600 keV Zr ions are shown on Figure 3. It can be seen that contrary to proton irradiation, the irradiated layer is very thin (between 150 to 300 nm thick) and only a thin part of the 6 µm grain is irradiated close to the free surface. The irradiated material cannot be considered as bulk material in that case, and free surface effects, such as point defects elimination on the surface, are believed to be significant.
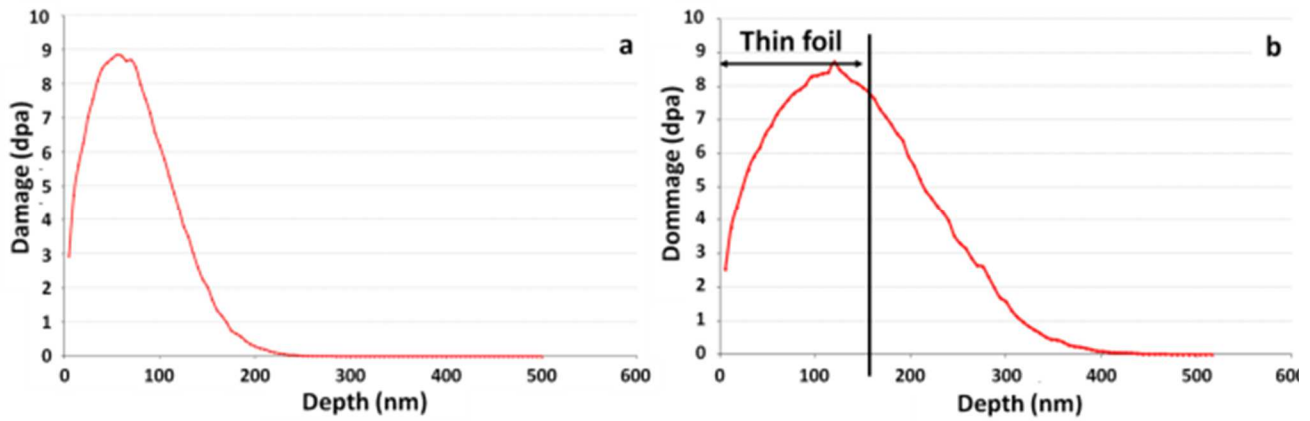
Figure 3 : TRIM calculations a) for 300 keV Zr ions in Zr 11.5×10¹⁴ ions/cm² , b) for 600 keV Zr ions in Zr, 11.5×10¹⁴ ions/cm² (E_d = 40 eV).

In order to apply an external stress on the samples, an original device, adapted for both facilities, has been designed (Figure 4). The samples are in the form of thin strips of 25 mm long, 1.9 mm wide and 0.1 mm thick. A four-point bending loading is applied on the samples (Figure 4). This loading geometry induces a pure shear stress state between the two central supporting points, inducing a pure tensile stress state on the thin irradiated layer of the samples. The stress level is deduced from the thickness of the sample h, its length L, the distance between the two central points, l, and the imposed displacement, u , between outer loading points and the inner loading points from Eq. 2.

$$\sigma_{irradiated\ area} = -\frac{6uEh}{(L-l)(L+2l)} \qquad (2)$$

16 samples can be irradiated at the same time, and various stress levels can be applied on the samples, thanks to modular central blocks with various displacements u . For each irradiation, several control samples are irradiated exactly in the same conditions but without any applied stress. The results obtained on samples irradiated under stress can be therefore always compared to control samples.
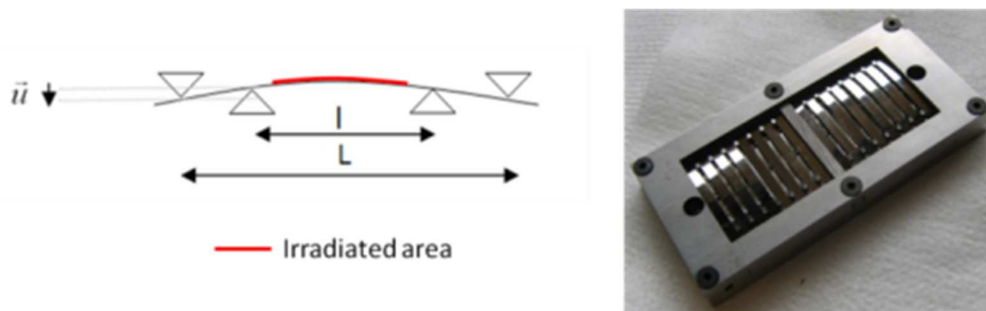
Figure 4 : Original device designed to apply a four-point bending loading under Zr ion irradiations.

Despite the poor thermal contact between the heating stage and the samples it has been checked, using a thermocouple welded on a sample, that for a given heating power, the irradiation temperature on the samples is 573 K. Furthermore, due to the very low power deposited per unit surface by the Zr ion beam (67 W/m²), there is no additional heating due to the ion beam. Because of the limited power of the heating stage and the poor thermal contact between the samples and the holder, it was not possible to conduct the irradiation with a specimen temperature higher than 573 K. Additional experiments are needed to identify the appropriate temperature shift to simulate PWR neutron irradiation.

The samples used here have been taken in the AD-TD plane, the long direction of the strip being either along the Transverse Direction (TD) or along the Axial Direction (AD). Before irradiation, the thin strips of 0.1 mm thick are electro-polished on one side either in a form of flat electro-polishing or in a form of shallow dimple. After irradiation 3 mm disks are punched out of the strips and the irradiated

surface is protected by a varnish. Electro-polishing on the rear side is then performed in order to obtain thin foils that are then observed by TEM.

The original device developed for this study induces a bending of the sample, with a constant displacement during the experiment. Therefore, the unirradiated side of the strip (99.7 µm thick) subjected to a stress gradient relaxes the applied stress through conventional thermally activated viscoplastic deformation mechanisms. This thermally activated stress relaxation is observed after the experiment thanks to a residual bending of the samples. Nevertheless, this stress relaxation in the unirradiated part of the sample remains limited. It is estimated, from residual bending measurements, that only 23% of the initial applied stress is relaxed during the experiment. This is in rather good agreement with the stress relaxation measured by Carassou et al. [54] using three-point bending experiments and thicker samples where only 14% of the applied stress is relaxed after 100 hours at 588 K.

On the other hand, in the 0.3 µm thick irradiated part of the sample, rapid stress relaxation occurs because of irradiation activated deformation mechanisms. It is shown by Carrassou et al. [54] that the applied stress is nearly fully relaxed (85% relaxed) after a fluence of 5×10^{24} n/m^2 irradiation in Materials Testing Reactor at 588 K. Assuming that the same relaxation applies for the layer irradiated with Zr ions, despite the complex two-layer structure of the sample, the stress is nearly fully relaxed after 1.25 dpa using the conversion factor given in [55]. This shows that the device used here can only apply a stress on the irradiated layer for a short irradiation period. Thanks to this device two different loading histories have been studied.

Loading history I :
During this experiment, the stress is applied from the beginning of irradiation. The initial applied tensile stress on the irradiated layer is about 125 MPa. This applied stress is assumed to be in the elastic domain, considering a yield stress of the order of 150 MPa at 573 K. The stress in the irradiated layer is assumed to decrease rapidly during the first dpa of the Zr ion irradiation. The irradiation is conducted up to 4.8 dpa. Only M5^{TM} samples taken in the Axial Direction (AD) have been studied in this experiment.

Loading history II :
During the second loading history, the samples are first irradiated without any applied stress up to 4.1 dpa at 573 K. Then the samples are moved on the specimen holder, so that a tensile stress is applied on the irradiated layer. The initial applied stress is considered to be in the plastic domain in that case (higher than 150 MPa). The stress then is assumed to decrease rapidly between 4.1 to 5.1 dpa. The irradiation is conducted up to 7 dpa on overall. Only RXA Zy-4 samples taken in the Axial Direction and in the Transverse Direction are studied in this experiment. A similar study conducted on M5^{TM} sample is still under progress.

It has to be pointed out that for both loading histories the high stress applied on the samples is not representative of the in-reactor applied axial stress on the guide tubes which is usually of the order of 30 MPa.

The irradiation conditions are summarized in Table 5. Control samples have also been irradiated in the same conditions. Furthermore, additional control samples irradiated up to various doses have also been studied. All the irradiation conditions for control samples are given in Table 6.

Table 5 : Irradiations performed to study the influence of an applied stress on c-loops.

Loading	Irradiation	Material	Total irradiation dose		Applied stress		Damage creation rate (dpa/s)	Flux (ions/cm²/s)	Duration (h)
			dpa	Ions/cm²	Stress	Direction*			
I	Zr^{2+} 300 keV 573 K	M5^{TM}	4.8	9.0×10^{14}	Elastic (stress~125 MPa)	AD	4.7×10^{-4}	8.8×10^{10}	2h50
II	Zr^{+} 600 keV 573 K	Zy-4 pre-irradiated at 4.1 dpa	7	1.15×10^{15}	plastic	AD and TD	4.6×10^{-4}	7.6×10^{10}	4h10

* AD = Axial Direction ; TD = Transverse Direction

Table 6 : Zr ion irradiation conditions conducted on control samples without any applied stress.

Facility	Ion	Energy	Dose		T (K)	Damage rate (dpa/s)	Flux (ions/cm²/s)	Duration
			dpa	ions/cm²				
ARAMIS	Zr^{+}	600 keV	4.1	6.7×10^{14}	573	4.6×10^{-4}	7.0×10^{10}	2h30
			5.5	9.0×10^{14}				3h20
			7	1.15×10^{15}				4h10
IRMA	Zr^{2+}	300 keV	4.8	9.0×10^{14}	573	4.7×10^{-4}	8.8×10^{10}	2h50
			6.2	1.16×10^{15}		4.9×10^{-4}	9.2×10^{10}	3h30

2.5 Optical microscopy after proton irradiation

Unirradiated hydrided samples, control sample and hydrided samples irradiated with protons, have been polished and etched with fluoridric acid in order to reveal the hydrides. Conventional optical microscopy has then been performed on the samples.

2.6 TEM analysis method after charged particle irradiation

TEM observations have been performed on Jeol 2100 and Jeol 2010 transmission electron microscopes, both operating at 200 kV with a LaB$_6$ filament. For each irradiation conditions several thin foils have been studied and for each thin foil several grains were analyzed. Every thin foil has been taken in the AD-TD plane in this study. Thanks to the texture of the material many grains have their c-axis close to the Transverse Direction. As a consequence, many grains can be easily tilted in the appropriate conditions to observe c-loops, that is to say in the diffraction condition with g=0002.
For each grain, several pictures are taken to cover most of the grain surface and in the grain many loops are analyzed. The number of c-loops per unit volume N_V and their mean diameters $< d >$ were measured using an interactive digital drawing tablet connected to Visilog software. The grain thickness was measured using Electron Energy Loss Spectroscopy. When the c-loops are very large and, as a consequence, are truncated by the thin foil surfaces, the linear density L$_v$, defined in Eq. 3, is used.

$$L_V \ (m^{-2}) = \frac{Total \ length \ of <c> loop \ segments \ measured \ (m)}{Total \ volume \ studied \ by \ TEM \ (m^3)} \qquad (3)$$

The orientation of each grain was determined by using diffraction pattern indexing and recording the tilt angles. The stereographic projection was then drawn for each studied grain. The Axial Direction of the tube was always located on the thin foil, and the thin foil was always orientated so that the Axial Direction is parallel to the primary tilt axis.
When a stress (σ) was applied on the specimen under irradiation, the angle (θ), between the tensile direction and the c-axis is measured on the stereographic projection. Then, the component normal to

the loop plane of the deviatoric stress tensor, $\sigma_s^{<c>}$, is then computed according the SIPA theory (Eq. 4). Loop densities and diameter are then plotted as a function of this component.

$$\sigma_s^{<c>} = \sigma \left(\frac{2}{3} cos^2\theta - \frac{1}{3} sin^2\theta \right) \qquad (4)$$

3. Results on the effect of an applied stress under Zr ion irradiation

3.1 Control samples after Zr ion irradiation

TEM observations performed on control samples irradiated with 600 keV Zr ions at 573 K, on the ARAMIS facility first show that the c-loop microstructure obtained in M5^{TM} and RXA Zy-4 are very similar (Figure 5). It is observed that the mean loop diameter increases from 24 to 36 nm from 4.1 to 7 dpa. The number density also increases from 2.9×10^{20} to 1.0×10^{21} m^{-3}. Similar results are obtained with 300 keV Zr ions, although a slight shift in number density can be noticed as shown on Table 7.
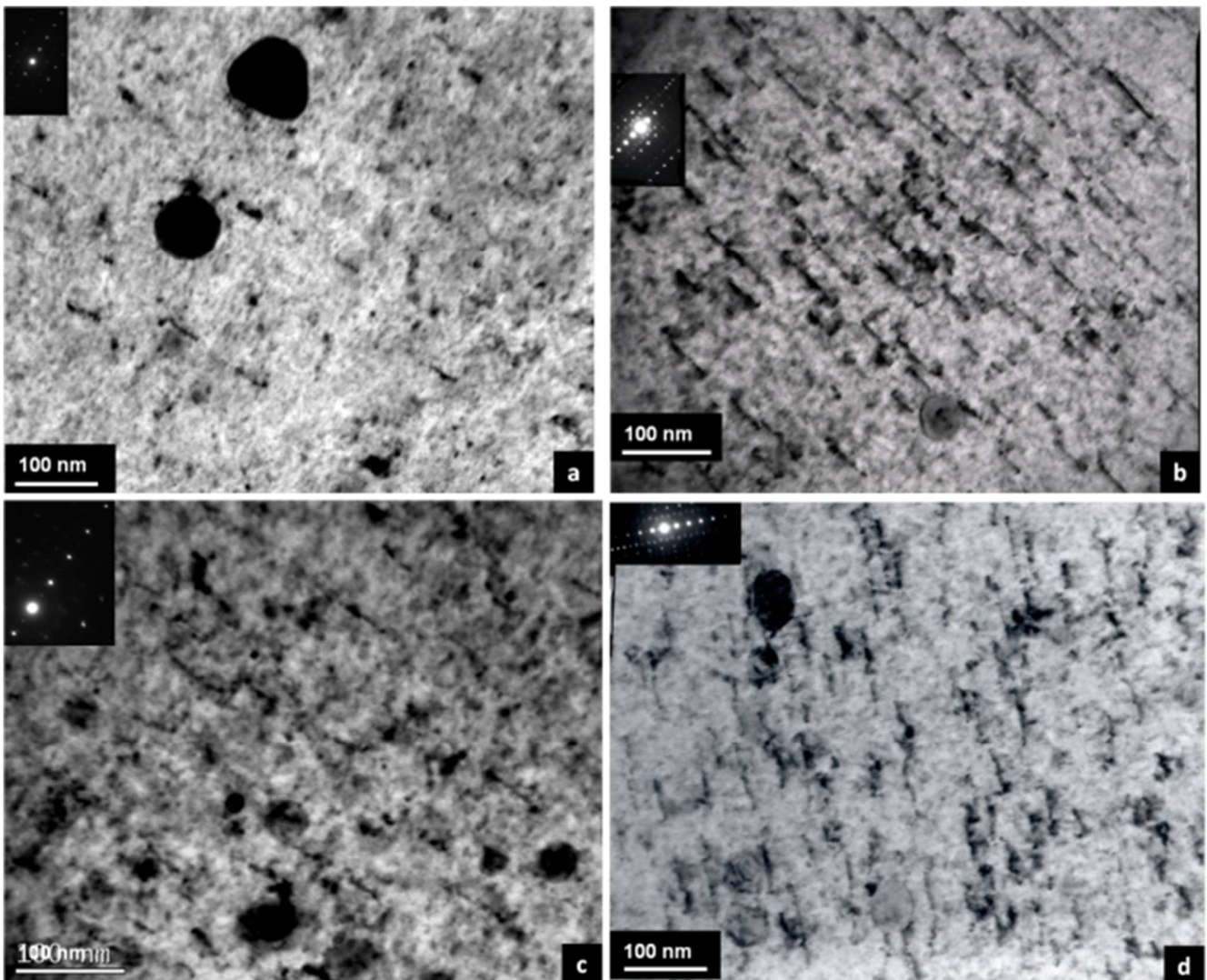
Figure 5 : c-loop microstructures observed after 600 keV Zr ions at 573 K on ARAMIS. a) RXA Zy-4 irradiated up to 4.1 dpa; b) RXA Zy-4 irradiated up to 7 dpa; c) M5^{TM} irradiated up to 4.1 dpa; d) M5^{TM} irradiated up to 7 dpa.

Table 7 : Mean loop diameter, number density and linear density of c-loops after irradiations conducted at 573 K on the IRMA and ARAMIS facilities respectively with 300 and 600 keV Zr ions.

Material	Energy	Dose (dpa)	Mean diameter (nm)	Number density (m^{-3})	L_v (m.m^{-3})	Number of loop analyzed
Zy-4	300 keV	6.2	35	1.6×10^{21}	5.7×10^{13}	525
Zy-4	600 keV	4.1	24	2.9×10^{20}	6.6×10^{12}	640
Zy-4	600 keV	5.5	26	6.7×10^{20}	1.6×10^{13}	1300
Zy-4	600 keV	7	36	9.1×10^{20}	3.3×10^{13}	1400
M5^{TM}	300 keV	4.8	19	2.5×10^{21}	5.0×10^{13}	1860
M5^{TM}	300 keV	6.2	43	1.9×10^{21}	8.7×10^{13}	475
M5^{TM}	300 keV	5.5	30	1.1×10^{21}	3.4×10^{13}	1100
M5^{TM}	300 keV	7	28	1.0×10^{21}	2.8×10^{13}	610

3.2 Stress applied at the beginning of Zr ion irradiation at 573 K

TEM observations performed on M5^{TM} specimens irradiated with 300 keV Zr ions under an applied stress (loading history I) up to 4.8 dpa show no influence of the stress when compared with control samples. Indeed, as illustrated on Figure 6, when plotted as a function of the component normal to the loop plane (along the c-axis) of the deviatoric stress tensor, no trend is observed concerning the loop number density or the loop mean diameter. This proves that there is no effect of an applied stress at the early stage of irradiation on c-loops.

Since M5^{TM} and Zy-4 control samples exhibit the same microstructures, it is assume that this result also applies for Zy-4 irradiated under stress.
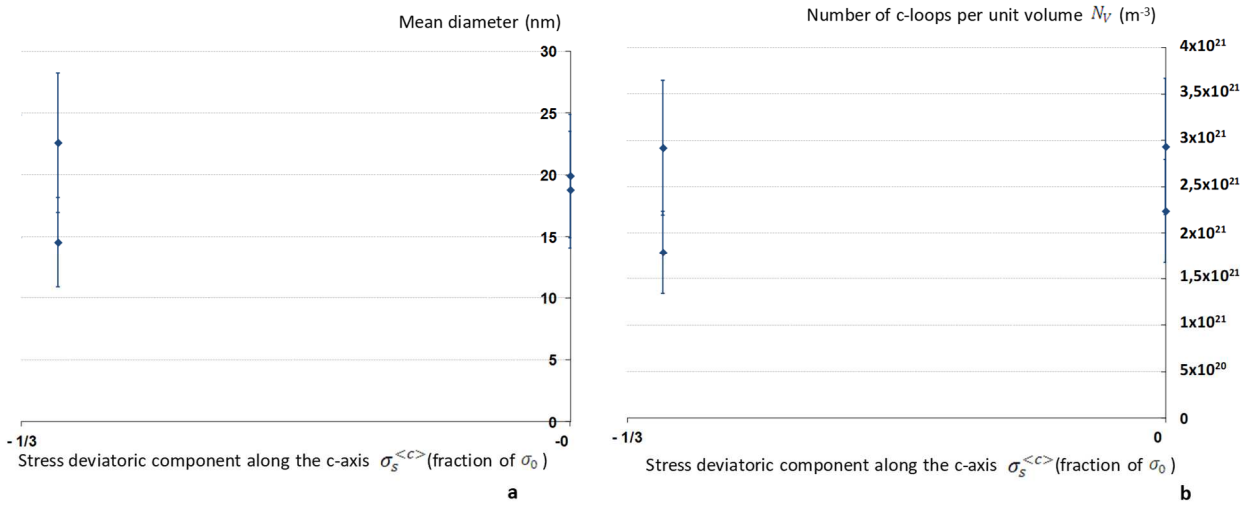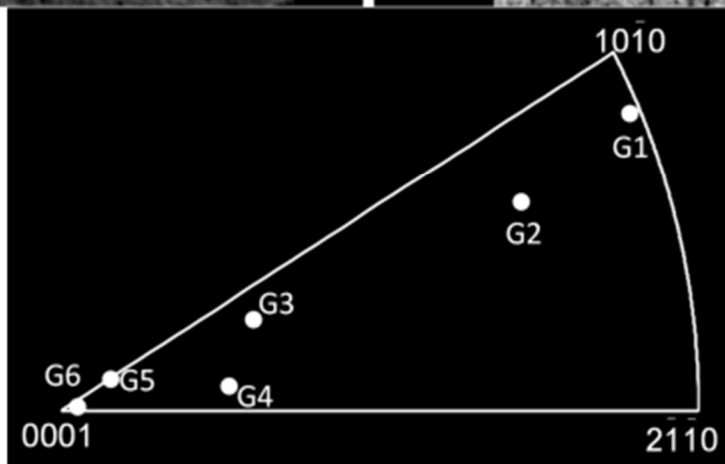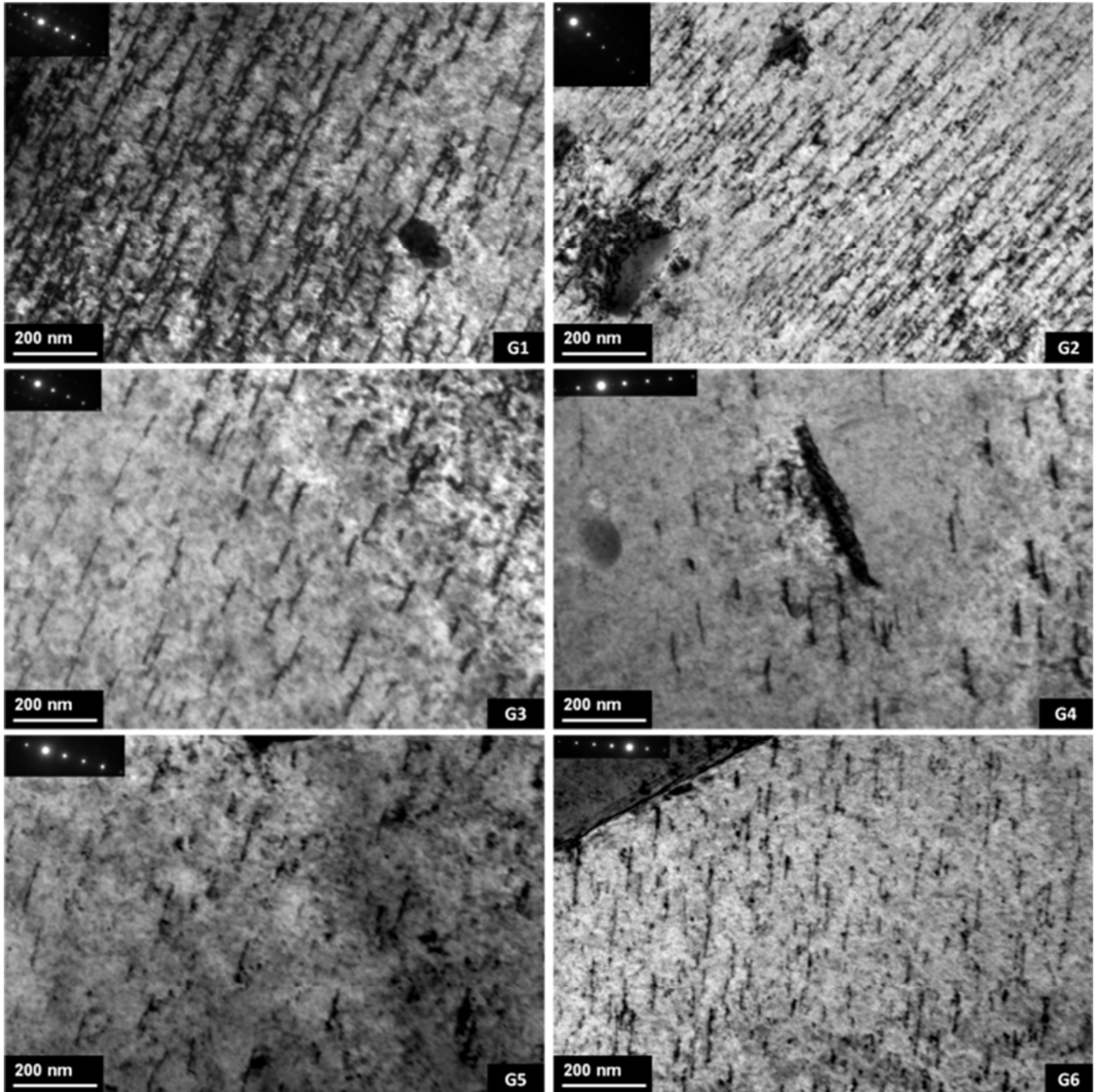

Figure 6 : M5^{TM} irradiated by 300 keV Zr ions at 573 K on IRMA up to 4.8 dpa. C-loop mean diameter and number density $N_{<c>}$ as a function of $\sigma_s^{<c>}$ (deviatoric stress component along the c-axis).

3.3 Stress applied after 4.1 dpa Zr ion irradiation at 573 K

TEM observations were performed on Zy-4 samples which have undergone the second loading history. TEM pictures are given in Figure 7. The number density, mean loop diameter and linear density are reported on Figure 8 and Figure 9 as a function of $\sigma_s^{<c>}$, the component normal to the loop plane (along the c-axis) of the deviatoric stress tensor. The mean values measured on control samples irradiated up to 7 dpa in the same conditions, but without any applied stress [56] are shown by a green cross on Figure 8 and Figure 9.

It is shown on Figure 8 that when a positive stress is applied along the basal plane, normal to the c-axis, the c-loop density (number density N_V and linear density L_V) is higher than when it is applied along the c-axis. On the other hand, the loop diameter seems to be not sensitive to the applied stress. Furthermore, TEM observations performed on control samples irradiated up to 4.1 dpa without applied stress show that c-loops are already present in the material in low density. This proves that if a stress is applied when c-loops start to nucleate and grow, their evolution is affected..

Figure 7 : c-loop microstructures observed in RXA Zy-4 irradiated by 600 keV Zr ions at 573 K after the second loading history. The stress direction is given in the crystal frame on the inverse pole figure.
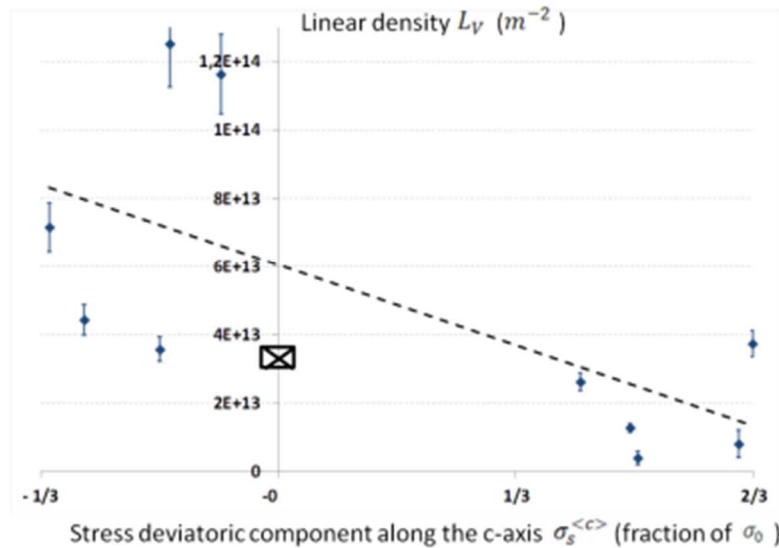
Figure 8 : RXA Zy-4 irradiated by 600 keV Zr ions at 573 K according to the second loading history (up to 4.1 dpa without any stress, during 2.9 dpa more under stress). C-loop linear density L_V as a function of the deviatoric stress component along the c-axis ($\sigma_s^{<c>}$). The cross on the ordinate axis corresponds to the mean value obtained for control samples.
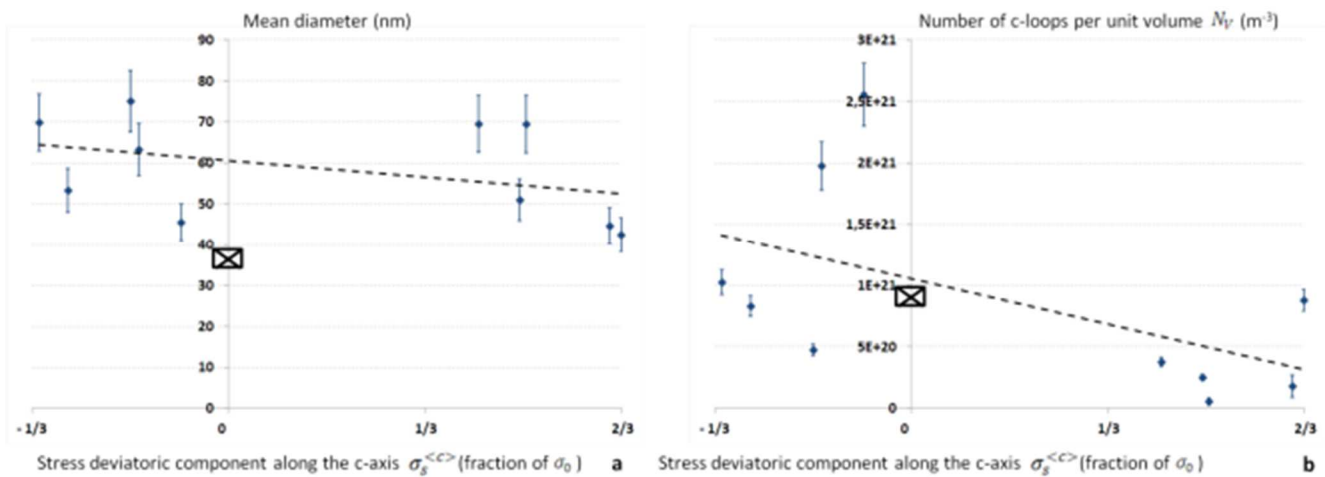

Figure 9 : RXA Zy-4 irradiated by 600 keV Zr ions at 573 K according to the second loading history (up to 4.1 dpa without any stress, during 2.9 dpa more under stress). a) C-loop mean diameter and b) number density as a function of $\sigma_s^{<c>}$. The cross on the ordinate axis corresponds to the mean value obtained for control samples.

4.   Results concerning the effect of hydrogen using proton irradiation

4.1   Optical microscopy and thermo-desorption results

First of all, optical microscopy observations performed on M5^{TM} control sample irradiated with protons up to 19 dpa show (Figure 10) that many small hydrides are present and homogeneously distributed in the sample thickness. This is consistent with the assumption of the rapid diffusion of the implanted hydrogen in the entire specimen. Nevertheless, a fine line located at 30 µm under the irradiated surface can be noticed on Figure 10. This "line" could be due to an enhanced hydride precipitation at the implantation and/or damage peak (located between 25 and 30 µm depth). It is also possible that preferential chemical etching occurs at damage peak because of the very high density of irradiation defects.
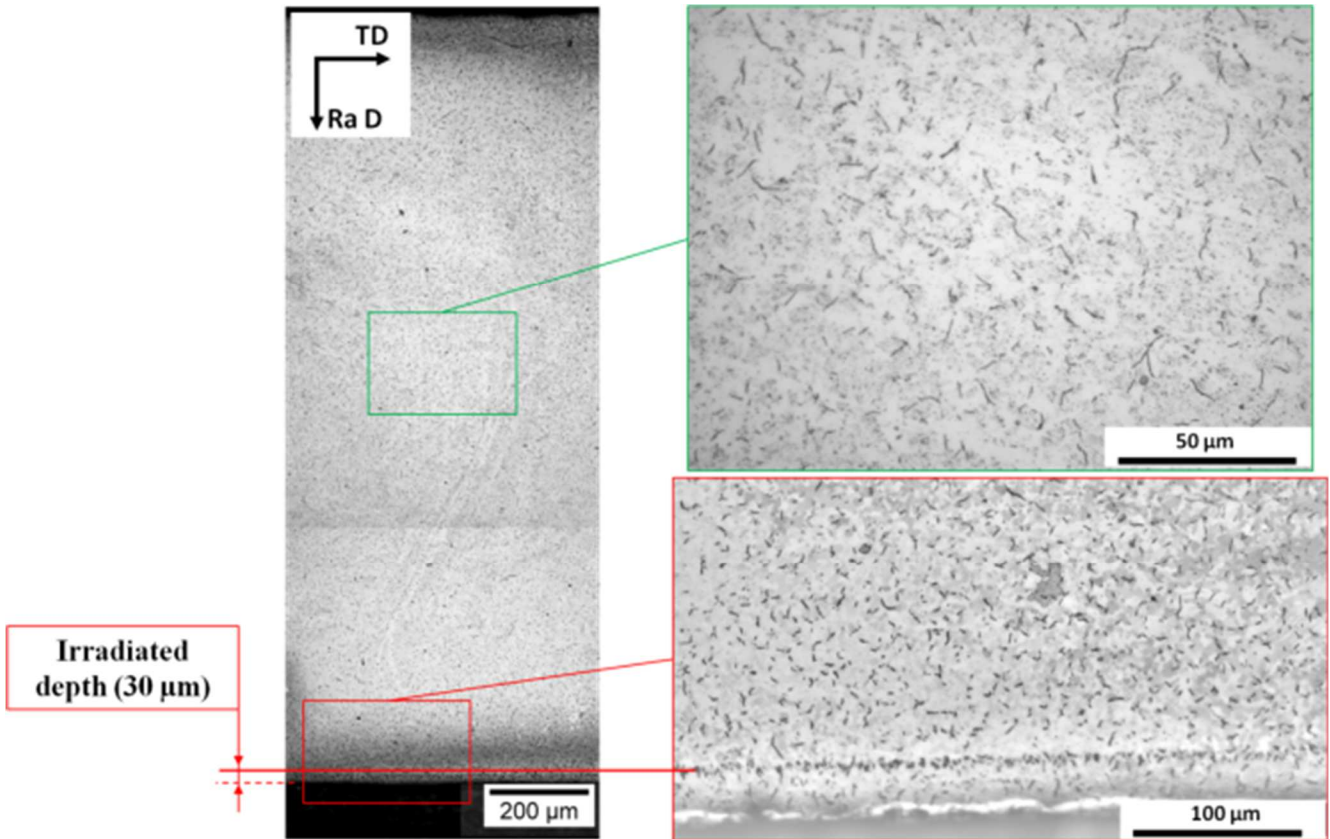
Figure 10: Hydrides precipitated in "as-received" M5^{TM} after a 19 dpa proton irradiation at 623 K. Optical Microscopy performed in the TD-ND plane (Normal or Radiale Direction).
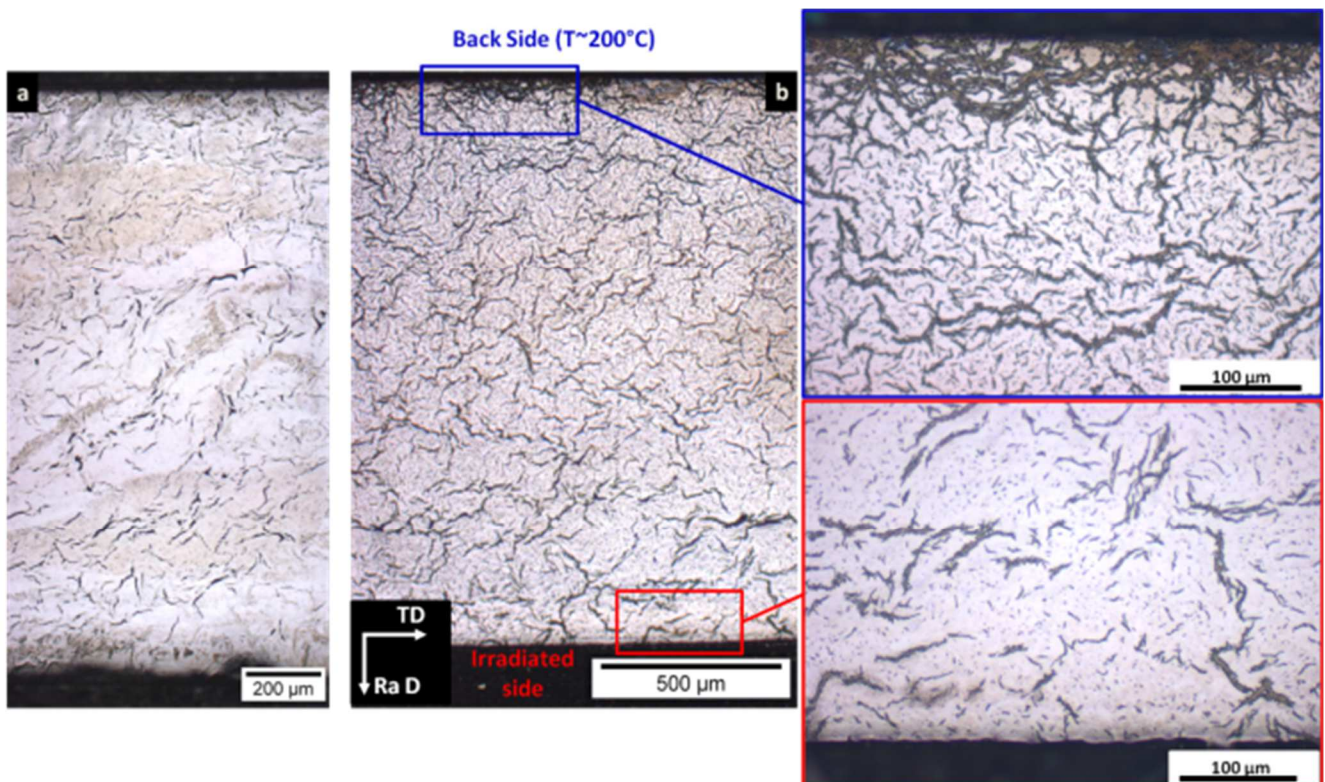
Figure 11 : 350 wppm pre-hydrided M5^{TM}. Optical microscopy observations in the TD-ND plane. a) before irradiation; b) after 2 MeV proton irradiation at 623 K up to 19 dpa.

Then, optical microscopy observations performed on pre-hydrided samples before irradiation show that hydrides precipitation is homogeneous and consistent with the hydrogen contents measured by thermo-desorption. The same thermo-desorption experiments, this time performed on a pre-hydrided

M5[TM] sample annealed during 200 hours at 623 K under secondary vacuum, prove that hydrogen desorption remains limited (less than 20 wppm).

However, after proton irradiation (260 hours at 623 K), a significant gradient of precipitated hydrides in the thickness of the sample can be noticed (Figure 11). Indeed, numerous precipitated hydrides are observed in the back of the sample. This phenomenon is probably due to the thermal gradient in the samples under protons irradiation. Indeed, because of the high power deposited by the proton beam on the irradiated surface, the temperature on the surface is 100 K higher than on the back of the sample which is in contact with the liquid indium. Since it is known that hydrogen diffuses towards colder areas [57], the hydrogen content is higher on the back of the sample than on the irradiated side. Nevertheless, optical microscopy and Transmission Electron Microscopy observations proved that hydrides are still present in significant amount in the 30 µm thick irradiated layer where TEM analysis are performed, but the local hydrogen content is not accurately known and is presumably lower than the overall hydrogen content estimated by adding the implanted hydrogen and the initial content.

4.2 TEM results: Control samples after proton irradiation

TEM observations have been performed on control samples in M5[TM] and RXA Zy-4 after proton irradiation. As described in a previous study [46] c-loops are observed after proton irradiation (Figure 12). The c-loop diameter and density are in rather good agreement with the observations performed after neutron irradiation (Table 8). The diameter is nevertheless slightly smaller than after neutron irradiation. Most remarkably, as for neutron irradiation, it is observed that after proton irradiation the c-loop density in M5[TM] is much lower than in RXA Zy-4.

Table 8 : Mean loop diameter, number density and linear density of c-loops after 2 MeV proton irradiation conducted at 623 K on Zy-4 and M5[**TM**] control samples. PWR results are also given in the table.

Irradiation and temperature	Material	Dose (dpa)	Mean diameter (nm)	Number density (m^{-3})	L_v $(m.m^{-3})$	Number of loop analyzed
Protons, 623 K	Zy-4	8,1	102	4.0×10^{20}	4.4×10^{13}	4133
Protons, 623 K	Zy-4	12,5	123	1.0×10^{21}	1.1×10^{14}	350
Protons, 623 K	Zy-4	19	111	1.1×10^{21}	1.3×10^{14}	1048
PWR, 583 K [26]	Zy-4	14	> 150 [a]	< 1.2×10^{21} [a]	1.8×10^{14}	
PWR, 593 K [40]	Zy-4 low Sn RXA	35	> 150 [a]	< 1.17×10^{21} [a]	1.75×10^{14}	
Protons, 623 K	M5[TM]	4,9	0	0	0	0
Protons, 623 K	M5[TM]	8,1	55	1.0×10^{20}	5.7×10^{12}	202
Protons, 623 K	M5[TM]	12,5	49	2.2×10^{20}	1.1×10^{13}	290
Protons, 623 K	M5[TM]	19	71	2.5×10^{20}	2.0×10^{13}	543
PWR, 593 K [40]	M5[TM]	29,1	> 150 [a]	< 2.3×10^{20} [a]	3.4×10^{13}	

4.3 TEM results: Impact of the hydrogen in M5[TM]

TEM observations have been performed on pre-hydrided M5[TM] sample irradiated with protons up to 19 dpa. When conducting TEM observations, two distinct areas of the grain have been analyzed successively: the surroundings of the hydrides and the others areas of the grain, the so-called "matrix", far from hydrides.

a- C-loops far from hydrides in M5[TM]

Firstly, only the results obtained in the "matrix" (far from precipitated hydrides) are reported. TEM observations were performed on M5[TM] samples pre-hydrided up to three different contents. These samples were irradiated by 2 MeV protons at 623 K up to 19 dpa. Measurements of c-loop densities have been done in the matrix, far from the precipitated hydrides (Figure 12). The densities obtained are given in Figure 13 as a function of the hydrogen content. These results tend to show a linear relationship between c-loop densities and the hydrogen content up to 350 wppm hydrogen.

Moreover, TEM observations have been conducted on 350 wppm pre-hydrided M5^{TM} after the four irradiation doses. These observations (Figure 12) show a higher c-loop density and a more homogeneous c-loop microstructure in the pre-hydrided samples than in the control samples. Indeed, in the control samples, c-loops are mainly observed at the vicinity of some precipitates and at grain boundaries [46]. Even if these phenomena are still observed in the pre-hydrided samples, c-loops are also present in the middle of the matrix, far away from the secondary phase precipitates and grain boundaries. Most remarkably, c-loops are observed after 4.9 dpa in the 350 wppm pre-hydrided samples whereas they are not present after the same irradiation dose on control samples. This proves that the pre-hydriding induces a shift toward lower doses of the threshold dose for c-loop nucleation. From these quantitative results (Figure 14), a c-loop evolution law, far from hydrides, could be proposed (Eq. 5). The threshold dose (ϕt_c) is equal to 4.36 dpa for 350 wppm pre-hydrided samples whereas it is equal to 5.55 dpa for control samples. The slope of the linear evolution (A) is equal to 3.92×10^{12} m^{-2}.dpa^{-1} for 350 wppm pre-hydrided samples whereas it is equal to 2.63×10^{12} m^{-2}.dpa^{-1} for control samples.

$$\begin{cases} \quad \text{If } \phi t < \phi t_c , \ L_{V<c>} = 0 \\ \text{If } \phi t > \phi t_c , \ L_{V<c>} = A(\phi t - \phi t_c) \end{cases} \quad (5)$$

To finish, in the 350 wppm pre-hydrided M5^{TM} samples irradiated up to 19 dpa, moiré fringes have been observed on c-loops (Figure 15). This contrast results probably from the presence of nano-particles precipitated on c-loops. Observation of these particles by HR-TEM shows that they are coherent with the Zr matrix with a little misfit. Such particles are not observed in the control samples coming from the same irradiation. It can be assumed that these particles are nano-hydrides precipitated under irradiation.

### b- C-loops in the surroundings of "hydrides" in M5^{TM}

In addition to the increase of c-loop density far from hydrides another peculiar feature has been studied by TEM. Some sort of c-loop bundles are observed, as shown on Figure 16 to Figure 18. On Figure 16 it is clearly seen that the c-loop bundle appears between two delta hydrides (with an OR2 orientation with the matrix). On Figure 16 to Figure 18, it can be noticed that the c-loop bundle exhibits a form very similar to hydrides, elongated along the basal plane. Furthermore, it is also observed that c-loop bundles are often associated with the presence of <c+a> dislocations. C-loop bundle formation has been confirmed by numerous observations performed on various samples irradiated different up to 19 dpa and pre-hydrided from 80 wppm to 350 wppm.

It is believed that these c-loop bundles are created close or at the location of partially or fully dissolved hydrides. Indeed, <c+a> dislocations could be the remaining accommodation dislocations that may be created around hydrides due to the high volume increase ($\Delta V / V = 17\%$) during hydride precipitation. The form of the bundles and the presence of c-loops between two partially dissolved hydrides also support this hypothesis.

On the other hand, it has been noticed that when a hydride is fully precipitated, that is to say not partially nor fully dissolved, no effect on c-loop is observed (Figure 19).

4.4 TEM results : impact of hydrogen on Zy-4

TEM observations have also been performed on pre-hydrided RXA Zy-4. Many c-loops are already observed in control sample in RXA Zy-4 (Figure 20). In pre-hydrided samples, no clear increase of c-loop density is observed (Figure 20).
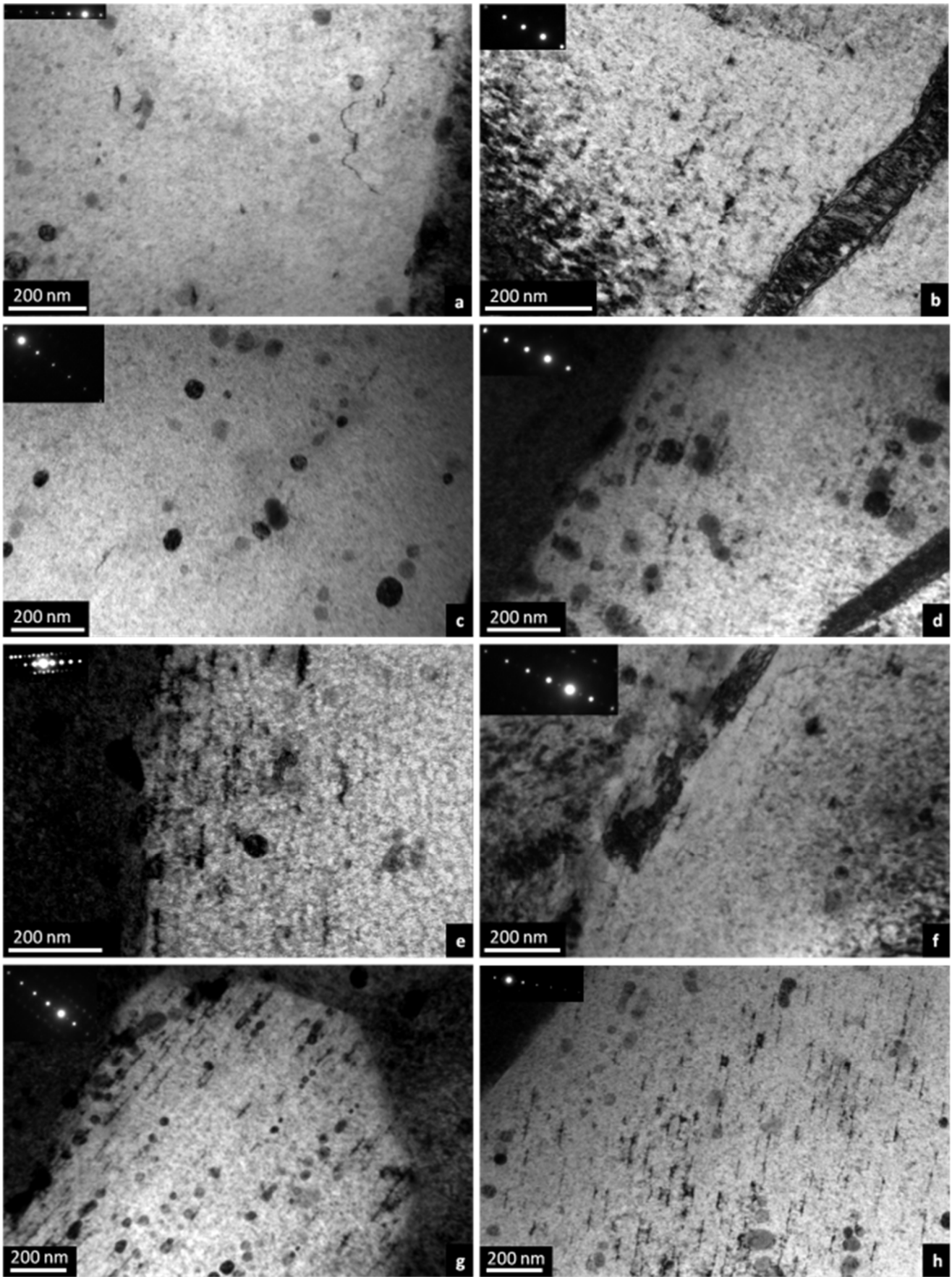
Figure 12 : C-loop microstructures observed in M5™ control samples (a) c) e) and g)) and 350 wppm pre-hydrided M5™ (b) d) f) and h)) after 2 MeV proton irradiations at 623 K up to : a) and b) 4.9 dpa ; c) and d) 8.1 dpa ; e) and f) 12.5 dpa ; e) and f) 12.5 dpa ; g) and h) 19 dpa.
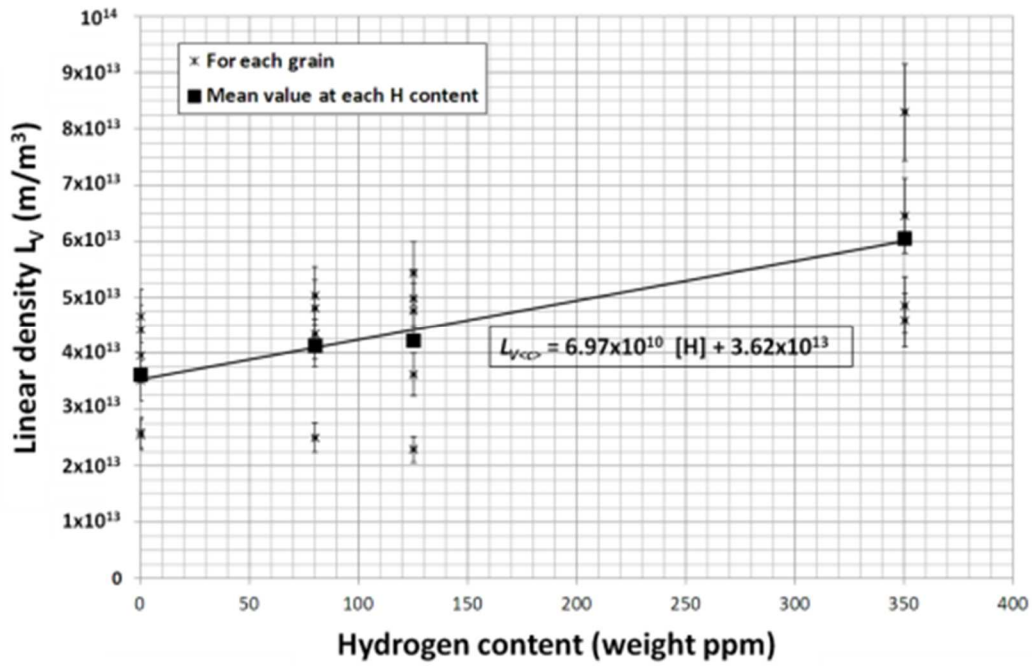
Figure 13 : C-loops linear density L_V evolution as a function of the initial hydrogen content. M5^{TM} irradiated by 2 MeV protons at 623 K up to 19 dpa.
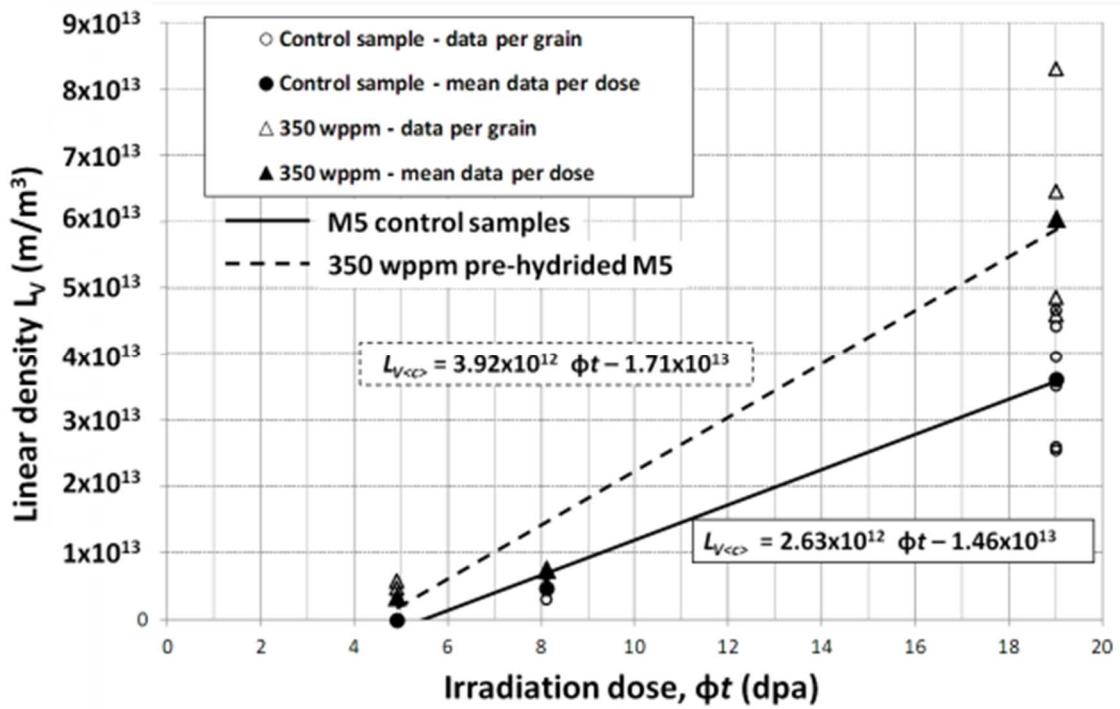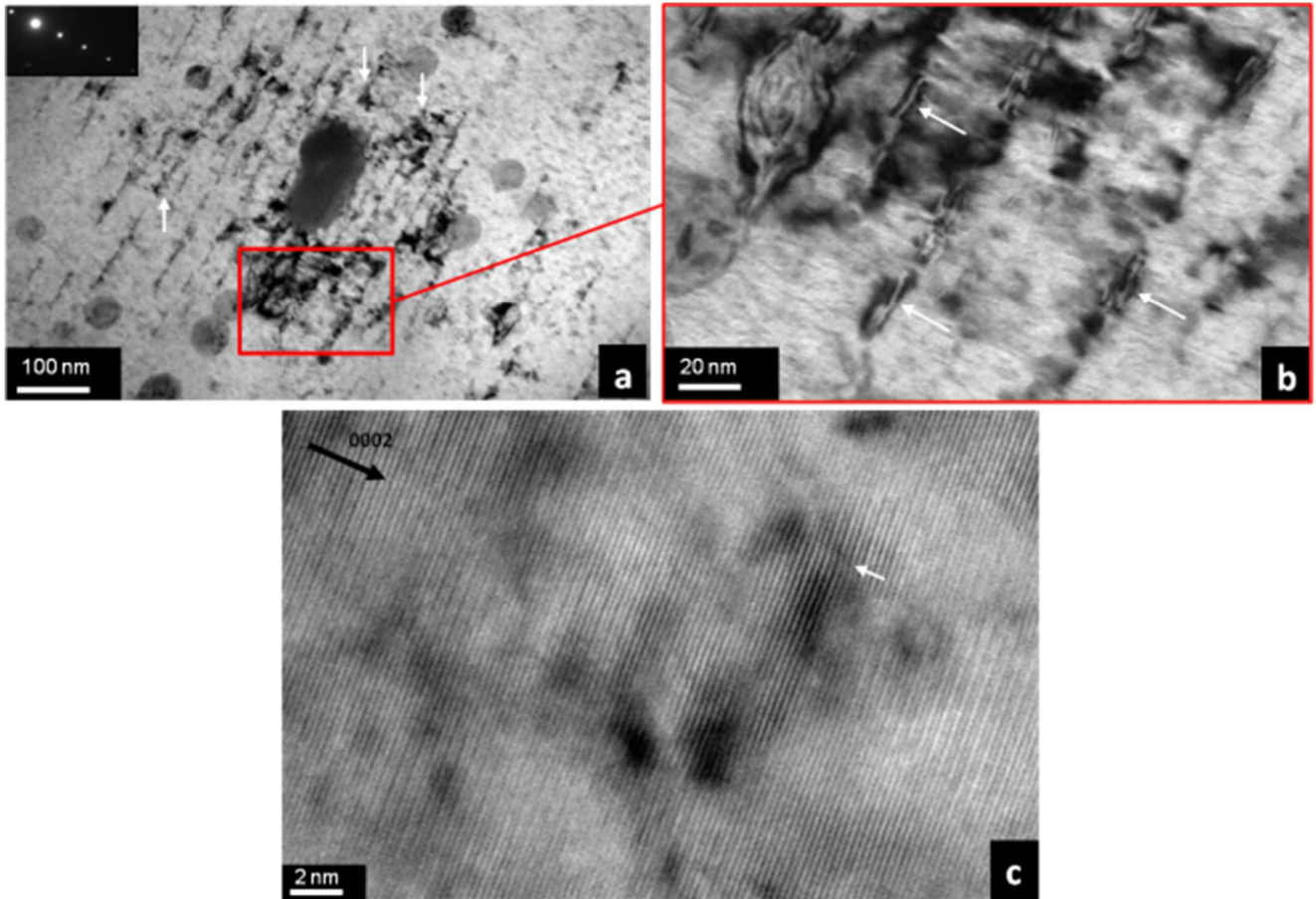

Figure 14 : C-loops linear density L_V in 350 wppm M5^{TM} and control samples as a function of the irradiation dose (dpa).

Figure 15 : Nano-contrast observed on c-loops in 350 wppm M5^{TM} samples irradiated up to 19 dpa with 2 MeV protons at 673 K. a) and b) "moiré" fringes; c) HR-TEM on a nano-particle.
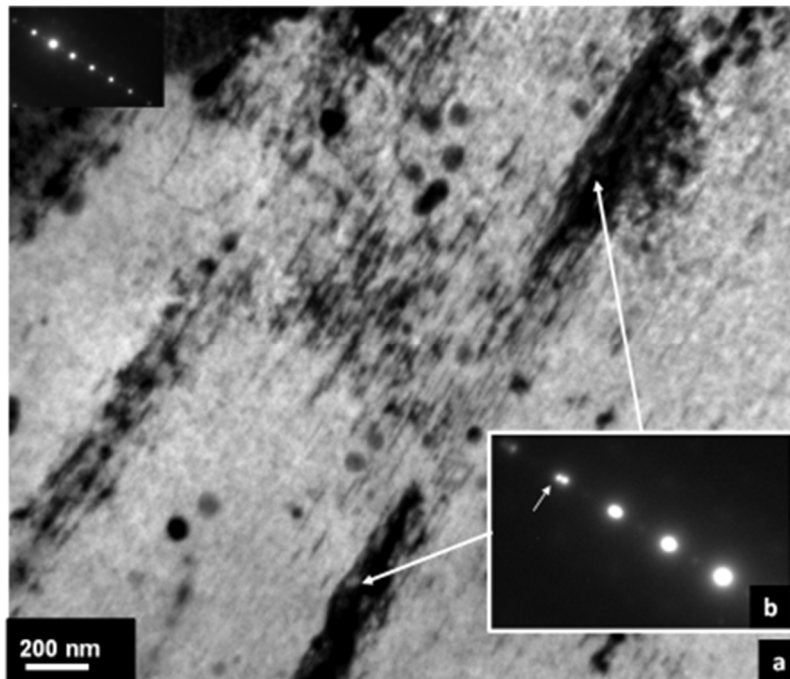
Figure 16 : 350 wppm pre-hydrided M5^{TM} irradiated by 2 MeV protons at 623 K up to 19 dpa. a) c-loop bundle at a vicinity of a partially dissolved hydride. b) Diffraction pattern of the precipitated hydride (OR2 orientation) for a $\underline{\boldsymbol{g}} = \boldsymbol{0002}$ diffraction vector.

Figure 17 : 350 wppm pre-hydrided M5™ irradiated by 2 MeV protons at 623 K up to 19 dpa. C-loop bundles a) <c+a> dislocations pointed by write arrows; b) the same picture at a higher magnitude.

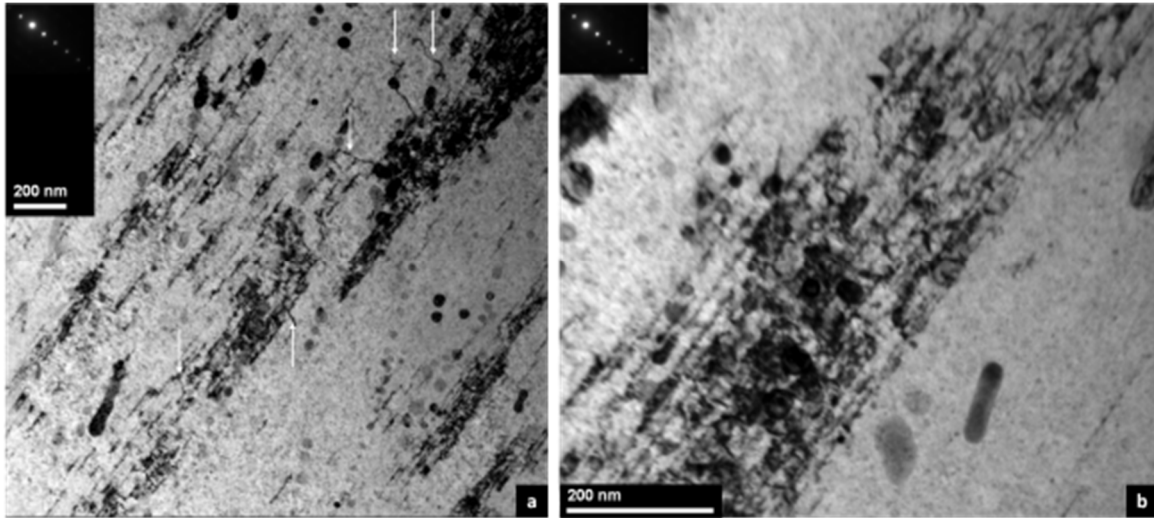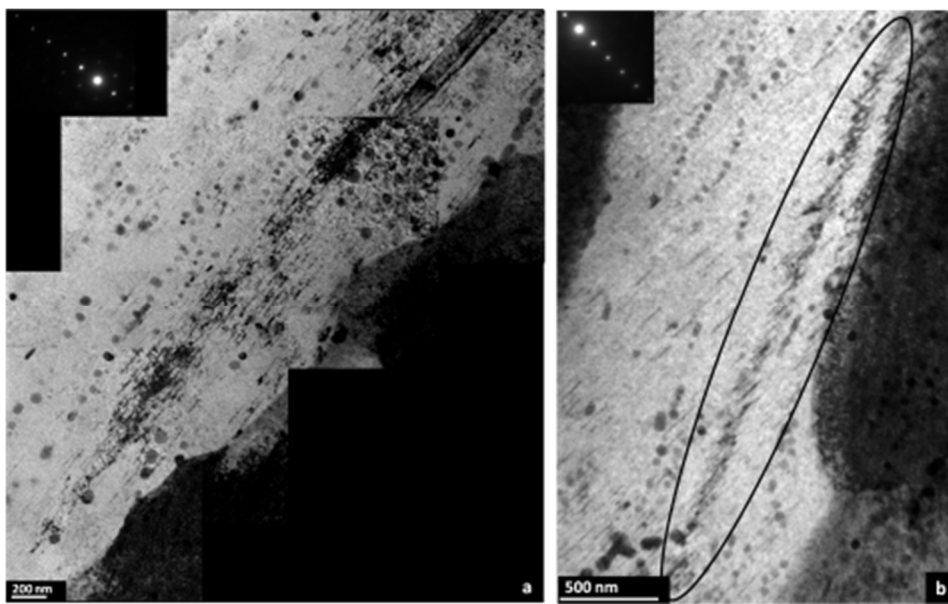**Figure 18 :** 80 wppm pre-hydrided M5™ irradiated by 2 MeV protons at 623 K up to 19 dpa. a) C-loop bundle on a former hydride precipitated in the basal plane and now completely dissolved; b) former hydride now completely dissolved.
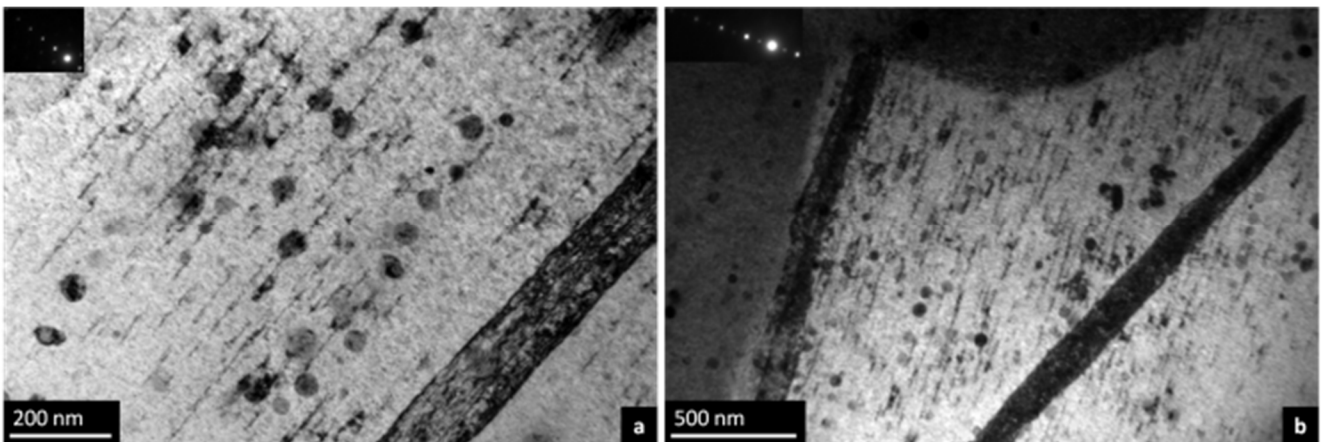
Figure 19 : M5™ irradiated by 2 MeV protons at 623 K up to 19 dpa. Observation at the vicinity of fully precipitated hydrides a) in 80 wppm pre-hydrided M5™; b) in 350 wppm pre-hydrided M5™.
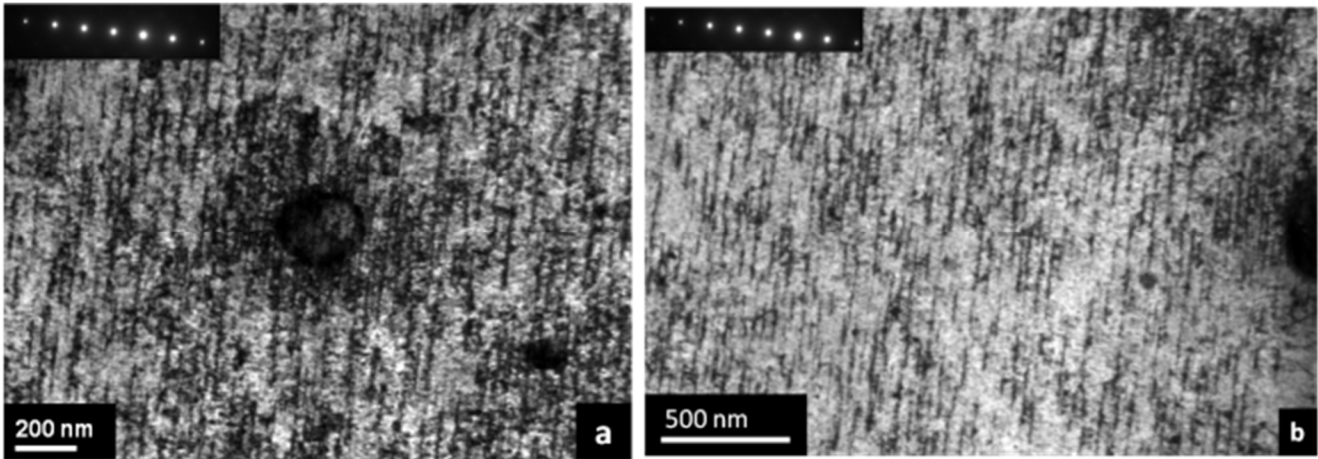
Figure 20 : RXA Zy-4 irradiated by 2 MeV protons at 623 K up to 19 dpa. a) control sample; b) 185 wppm pre-hydrided sample.

5. Discussion

Under irradiation, point defects are created in displacement cascades. These point defects migrate and cluster together leading to the creation of point defect clusters in the form of <a> and c-loops in zirconium alloys [3]. The evolution of <a> loops and c-loop diameter and number density depend on the absorption and emission of point defects by the loops and also by the other sinks present in the material. The evolution of the microstructure under irradiation can be simulated using cluster dynamics modeling [27, 58]. In this framework, loop nucleation and growth is governed by the net flux of point defects on loop. A vacancy loop can nucleate and grow if the flux of vacancies absorbed by the loop is higher than the sum of the flux of self-interstitial atoms (SIA) absorbed and the flux of vacancies emitted by the loop. Because of the high formation energy of self-interstitial atoms, point defect clusters cannot emit SIA. Thus, the resulting c-loop microstructure, and therefore the resulting free growth, depends on the emission and capture rate of point defects by c-loops. The differences observed between the c-loop microstructures obtained after various types of irradiation can be explained by considering the balance between emission and capture rate of point defects.

The influence of the applied stress or of the hydrogen content can also be interpreted by considering their potential effects on the absorption or capture rate of point defects by c-loops.

5.1 Discussion on the differences between the various irradiation types

For 300 keV or 600 keV Zr ion irradiation, displacement cascades are large, as for PWR neutron irradiation [59] as shown by the weighted recoil spectra given in [46]. However, for transferred energies higher than 10 keV, these large cascades break into sub-cascades. On the other hand proton irradiation displacement cascades are very small as shown by the weighted recoil spectra given in [46]. This difference in the primary damage morphology could have significant effects on the microstructure evolution under irradiation. Indeed, in cascades small point defect clusters can be formed which can constitute nuclei for loops such as c-component loops. However, recombination of point defects occurs [59] leading to a lower fraction of defects available to migrate. As a consequence, for the same given dose in dpa, Zr ion irradiations are less efficient than for proton irradiation. In this respect, Zr ion irradiations should better simulate neutron irradiations than proton irradiations. Nevertheless, TEM observations have shown that the c-loop microstructure obtained after proton irradiation is representative of the one obtained after neutron irradiation. This proves that the primary damage morphology has not a significant effect on c-loop microstructure [15, 46].

On the contrary the damage rate seems to play a major role on c-loop microstructure. Indeed, for Zr ion irradiation, the damage rate is high (5×10^{-4} dpa/s), leading to a high concentration of point defects in the material, considering that the steady state has been reached. Therefore the nucleation rate of

point defect cluster nuclei, such as di-vacancies clusters, is significantly higher than the emission rate of vacancies by the nuclei. Indeed, the clustering rate of two single vacancies is proportional to the square of the vacancy concentration. A detailed derivation of the nucleation rate is reported by Was [59]. This author also states that higher vacancy production rates promote greater vacancy concentration and a higher cluster nucleation rate. This therefore explains that the nucleation rate of c-loops is higher under Zr ion irradiation resulting in a higher density of small c-loops as observed by TEM after Zr ion irradiation. On the other hand, for proton irradiation, the damage rate is lower (1.50×10^{-5} dpa/s), leading to a lower concentration of point defects in the material. This induces a lower capture rate of point defects by cluster nuclei, the emission of vacancies remaining the same, leading therefore to a lower nucleation rate. The c-loop density is thus lower and these fewer loops absorb the point defects present in the material, explaining the larger diameter of c-loops observed after proton irradiation.

It is difficult to explain, in this framework, the origin of the incubation dose observed for the nucleation of c-component loops. It is proposed here that the transition from E-type c-loop to I_l-type c-loop could be one of the origins of the incubation dose observed. Indeed E-type loop nuclei could exhibit a very low growth rate but as soon as I_l-type loops are formed, beyond a critical radius, they grow rapidly. The fact that the critical loop size for the transformation from E-type loop to I_l-type loop can be influenced by impurity content, according to [22], through its effect on the stacking fault energy, could also explain the strong sensitivity to alloying elements (Nb, Sn, Fe) observed in this study when comparing c-loops in M5^{TM} and RXA Zy-4 irradiated with protons. Additional numerical work is however needed to conclude on this point. It is also possible, as proposed in [14, 27], that because of diffusion coupling between vacancies and solute atoms, such as iron, heterogeneous precipitation occurs on point defect clusters. This type of phenomenon is observed in steels using Tomographic Atom Probe [60, 61]. This could also play a significant role on the incubation dose of c-loops in zirconium alloys.

The fact that no effect of alloying elements is observed for Zr ion irradiation could be explained by considering that during the 4 hours Zr ion irradiation at 573 K alloying elements do not have the time to diffuse toward the loop and therefore do not affect the loop nucleation and growth.

5.2 Discussion on the effect of stress

According to the SIPA mechanism described in details by Garner [31, 32] and Wolfer [33] the applied stress affects the capture efficiency of SIAs with respect to vacancies, which is characterized by the bias (Z_i^d). Indeed, it is known that the interaction energy between a straight dislocation and a SIA is higher than between a dislocation and a vacancy (Elastic Interaction Difference, EID) leading to a bias higher than one ($Z_i^d > 1$, usually a value of $Z_i^d = 1.1$ is used for Zr [58]), the bias used for vacancy being equal to one ($Z_v^d = 1$). For a dislocation loop, the bias also depends on radius R of the loop $Z_i^l(R) = Z_i^d f(R)$, where the function $f(R)$ can be found in [33, 58, 62].

In presence of other unbiased sinks, the flux of SIAs toward dislocations will therefore be higher than the vacancy flux. Because of the Difference in Anisotropic Diffusion (DAD) of point defects (faster migration of SIAs along the basal plane than along the c-axis) dislocations in the basal plane, such as c-component loops, absorb more vacancies than SIAs. Following Woo's approach [28] this phenomenon induces a geometrical bias that multiplies the bias due to EID. In the case of straight dislocation in the basal plane, the bias becomes lower than unity ($Z_i^d < 1$). This is also true for loops in the basal plane [27] leading to growth of vacancy c-loops.

When a stress is applied, the bias due to EID is modified according to Eq. 6.

$$Z_i^l(\sigma) = Z_0 + C\sigma_{ij}^s n_i n_j \qquad (6)$$

Z_0 is the EID bias without an applied stress, C is a constant which depends on the material and on the loop size. σ_{ij}^{0S} is the deviatoric stress tensor. n_i are the unit vector components which describe the vector normal to the loop habit plane. For a loop in the basal plane Eq. 6 can be rewritten as Eq. 7.

$$Z_i^l(\sigma) = Z_0 + C\sigma_s^{<c>} \qquad (7)$$

Where $\sigma_s^{<c>}$ is the component of the deviatoric stress tensor along the c-axis,

For tensile stress (σ) applied along the c-axis, it can be seen that : $\sigma_s^{<c>} = 2\sigma/3$ and the bias is equal to Eq. 8.

$$Z_i^l(\sigma) = Z_0 + \frac{2}{3}C\sigma \qquad (8)$$

From this formula it can be seen that a tensile stress applied along the c-axis increases the capture efficiency of SIAs compared to vacancies, leading therefore to a reduced growth of vacancy c-loop.

On the other hand when the stress is applied along the basal plane, $\sigma_s^{<c>} = -\sigma/3$ and the bias is expressed as Eq. 9.

$$Z_i^l(\sigma) = Z_0 - \frac{1}{3}C\sigma \qquad (9)$$

In that case the applied stress decreases the capture efficiency of SIAs compared to vacancies thus increasing the vacancy loop growth.

The results obtained on c-loop observed in several grains with various orientations are well explained by the SIPA mechanism. Indeed it can be seen on Figure 8 that when the deviatoric stress component along the c-axis is close to $2\sigma/3$ (tensile stress along c-axis) the number density of c-loops (N_V) is lower than the number density measured without an applied stress. On the other hand, when the deviatoric stress component along the c-axis is close to $-\sigma/3$ (tensile stress along the basal plane), the number density of c-loop increases and becomes significantly higher in some grains than the control samples without applied stress. The effect on the linear density is also significant despite the dispersion of the results. The mean loop diameter appears to be only slightly affected by the applied stress, in good agreement with the results and the analysis given by Garner et al. [31] and Wolfer [33]. It has also been checked, by limiting the analysis to grains with c-axis close to the surface of the foil that the observed effect is not due to differences in orientation of the c-axis with respect to the foil surface. From these results it can be deduced that when the stress is applied when c-loops start to nucleate and grow, the applied stress affects the loop growth thanks to the SIPA mechanism.

On the other hand the experimental results show that for the first loading history, no effect of stress on c-loops is observed. In this case the stress decreases rapidly in the irradiated area (85% relaxed after 1.25 dpa), the applied stress is close to zero when the first c-loops are clearly observed by TEM (with diameter larger than 5 nm). This observation suggests that at the beginning of irradiation (when the stress is applied) no c-loop nuclei are created or these nuclei are too small to be affected by the stress.

This phenomenon, observed here for the first time concerning c-loops, could have a significant impact on the in-reactor deformation of PWR fuel assemblies made of Zr alloys.

5.3   Discussion on the effect of hydrogen

Before irradiation, the hydrogen content in the pre-hydrided M5™ and RXA Zy-4 specimens is completely precipitated as hydrides since hydrogen solubility limit at room temperature is less than 20 wppm. At 623 K, the hydrogen solubility limit is 130 wppm [42, 63]. Thus, in the case of the 80 and 125 wppm pre-hydrided M5™ samples, during irradiation, all the hydrogen is in solid solution. These samples allow studying the role played by hydrogen in solid solution. On the other hand, for the 350 wppm pre-hydrided M5™ and the 185 wppm pre-hydrided Zy-4, some hydrides remain during

irradiation. These samples permit to observe both the effect of hydrogen in solid solution and the effect of hydrides remaining precipitated during the irradiation.

In the following the role played on c-loops by hydrogen in solid solution will be first discussed. Then, the role on c-loops of hydrides precipitated before or during the irradiation will be addressed.

a- Effect of hydrogen in solid solution

Ab initio computations performed at atomic scale have shown that hydrogen atoms decrease the basal stacking fault in α-zirconium [64]. Indeed Domain et al. [64], by studying the effect of hydrogen on dislocation glide, have shown that when 25% of tetrahedral sites on the stacking fault plane are filled by hydrogen atoms, the I_2 basal stacking fault excess energy decreases from 200 mJ/m^2 down to 80 mJ/m^2. This shows that segregation of hydrogen on stacking fault is likely to occur. Furthermore, when more than 40% tetrahedral sites are filled, the stacking fault excess energy becomes negative. This suggests, according to [64], that high local hydrogen content can even induce a stacking fault. Assuming that hydrogen also decreases the I_1 basal stacking fault energy, the c-loop energy, given in Eq. 1, is decreased by the presence of hydrogen atoms.

In the framework of cluster dynamics modeling [58], the vacancy emission rate by a vacancy loop, α_{nv}^v, is function of the binding energy between a vacancy and a loop (E_{nv}^B) according to Eq. 10.

$$\alpha_{nv}^v \propto \exp\left(-\frac{E_{nv}^B}{kT}\right) \quad (10)$$

Where k is the Boltzmann constant and T the temperature. This binding energy, which is a positive quantity, is defined by Eq. 11.

$$E_{nv}^B = E_v^f - \left(E_{nv} - E_{(n-1)v}\right) \quad (11)$$

Where E_v^f is the vacancy formation energy, E_{nv} the energy of the loop containing n vacancies, and $E_{(n-1)v}$ is the energy of the loop containing n-1 vacancies.

Using the loop energy based on elastic theory (Eq. 1), a first order approximation [62] can be obtained for the binding energy (Eq. 12).

$$E_{nv}^B \cong E_v^f - \frac{1}{2}\frac{V_{at}}{R\pi b}\left(2\pi\frac{\mu b^2}{4\pi(1-\nu)}ln\left(\frac{4R}{r_0}\right) + 2\pi R\gamma_{fault}\right) \quad (12)$$

Where V_{at} is the atomic volume. From Eq. 12, it can be seen that a decrease in the stacking fault energy, because of the presence of hydrogen atoms, induces an increase in the binding energy and therefore a decrease of the emission rate of vacancies by vacancy loops. As a consequence c-loop nucleation and growth rate are increased by the presence of hydrogen in solid solution. This phenomenon would be enhanced by segregation of hydrogen atoms on the loop stacking fault disk.

It is also possible, according to some authors [65, 66], that hydrogen atoms creates a Cottrell atmosphere around the dislocation line of the edge loop leading to a screening of the stress field and therefore to a decrease of the line energy of the loop. This phenomenon could also lead to an increased nucleation and growth of c-loops, as for the stacking fault energy.

The possible precipitation of nano-hydrides on c-loops in 350 wppm M5^{TM} irradiated up to 19 dpa could be mentioned as an experimental evidence for hydrogen trapping by c-loops.

These two mechanisms therefore explain the enhanced nucleation and growth of c-loops far from hydrides. The trapping of hydrogen atoms around dislocation lines (for both a-type and c-type loop) and on the stacking fault disks (only for c-loops) could also explain the increased apparent solubility of hydrogen in irradiated Zr alloys [41-43].

The linear evolution of the c-loop linear density with hydrogen content (Figure 13) above 130 wppm hydrogen is rather surprising since for contents above the solubility limit at 623 K, the solid solution content remains constant, by definition. This surprising phenomenon could be explained first by the increase of the apparent solubility under irradiation but also, by the fact that the local hydrogen content in the irradiated area is lower than the overall hydrogen content due to the temperature gradient in the samples. Furthermore it has also to be kept in mind that a significant amount of hydrogen is introduced in the material by the proton beam. In the case of the 350 wppm pre-hydrided samples irradiated up to 19 dpa, the overall hydrogen content after irradiation is of the order of 450 wppm. Considering that the hydrogen gradient is linear and that the hydrogen content is roughly three times higher in the cold side than in the irradiated side (qualitatively estimated from optical microscopy observations), the hydrogen content in the irradiated layer could be approximately of the order of 230 wppm only. From the data given by Vizcaino et al. [42] it can be estimated that at 623 K the hydrogen apparent solubility limit is around 230 wppm after irradiation instead of 130 wppm. In that case, the local hydrogen content in the irradiated layer would be close to the apparent solubility limit. The observation of few partially dissolved hydrides suggests that the local hydrogen is slightly higher than the apparent solubility limit. This can therefore explain that the c-component loop density increases when the hydrogen content during pre-hydriding is increased since the higher local hydrogen content is believed to be only slightly higher than the solubility limit. Nevertheless, further analysis is needed to have an accurate measurement of the local hydrogen content in the irradiated layer and then provide a thorough understanding of the results.

b- *Effect of hydrogen in the form of hydrides during irradiation*

Because of the increase of the apparent hydrogen solubility limit due to hydrogen trapping on irradiation defects and of hydrogen migration toward the cold area, the remaining hydrides are dissolved progressively during the proton irradiation. The hydrides act as source of hydrogen which migrate progressively and can be trapped by c-loops nuclei enhancing their growth. This could therefore explain the high c-loop density around dissolved or partially dissolved hydrides.

Another mechanism could also be proposed to explain some experimental results. Indeed, <c+a> dislocations have been observed on some c-loop bundles. These <c+a> dislocations are believed to be accommodation dislocations that are created because of the large volume increase ($\Delta V/V = 17\%$) due to hydrides precipitation. Indeed, it is described by several authors [67, 68] that a-type dislocations nucleate during the precipitation of small hydrides. Growth of large hydrides could also result in the nucleation of <c+a> dislocations although further investigations are needed to confirm this point.

As shown by Griffiths et al. [30, 69] these <c+a> dislocations could be nucleation sites for c-loops. Indeed, it is proposed here that a kink (of edge character) contained in the basal plane on a <c+a> dislocation (of screw character), with Burgers vector $\frac{1}{3}[11\bar{2}3]$, can dissociate into two partial dislocations with Burgers $\frac{1}{6}[02\bar{2}3]$ and $\frac{1}{6}[20\bar{2}3]$ (Eq. 12) (Figure 21). This creates a stacking fault ribbon of I_1 type. Such dissociation has already been discussed concerning plasticity mechanisms in zinc and zirconium [70, 71].

$$\frac{1}{3}[11\bar{2}3] \rightarrow \frac{1}{6}[02\bar{2}3] + \frac{1}{6}[20\bar{2}3] \quad (12)$$

Under irradiation one, or both, of these partial dislocations absorb more vacancies than SIAs since they are in the basal plane. As a consequence, they climb and the stacking fault ribbon widens resulting in the formation of a c-loop (Figure 21).
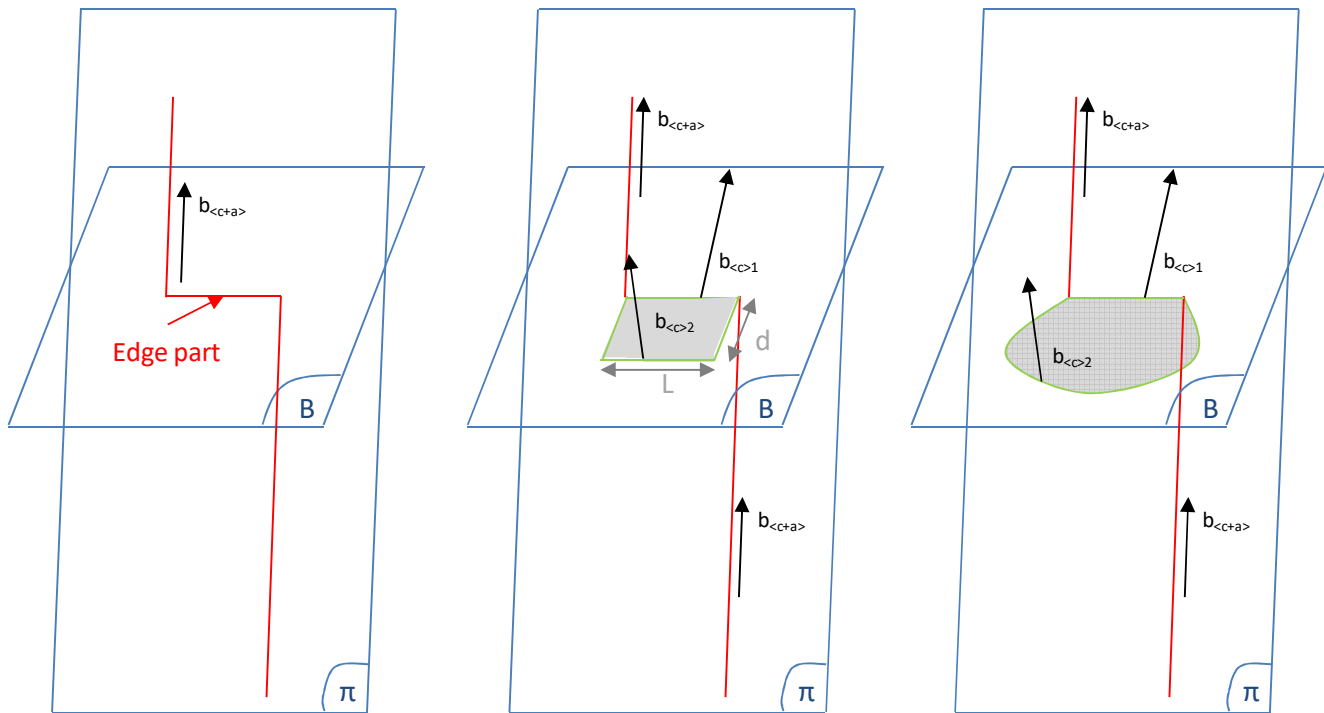
Figure 21 : Dissociation of a screw <c+a> disslocation in two partial dislocations with a c-type burgers vector separated by a stacking fault ribbon.

The observation of c-loop bundles in 80 wppm M5^{TM} is an experimental evidence of this mechanism. Indeed, in this material, all the hydrides are dissolved at irradiation temperature and only the <c+a> accommodation dislocations remain. Thus, the bundle formation could be explained only by the fact that these <c+a> dislocations act as nucleation sites for c-loops.

It has been pointed out that around fully precipitated hydrides, there is no increase in c-loop density nor c-loop bundle. This could be explained by considering that these hydrides have precipitated during the cooling down, after proton irradiation. It is also possible that some hydrides present during irradiation did not dissolve and therefore did not affect the c-loop evolution.

The impact of hydrogen on c-loops observed here for the first time, could have a significant impact on the in-reactor deformation of PWR fuel assemblies made of Zr alloys.

6. Conclusions

This experimental study first shows the relevance of using ions, such as protons or Zr ions, to simulate neutron irradiation and perform thorough analytical study on c-loops. Indeed, 2 MeV proton irradiations conducted at 623 K allow reproducing qualitatively and quantitatively the c-loop microstructures obtained in PWR operating conditions for the two studied alloys: M5™ and RXA Zy-4. Especially, some phenomena are also observed after proton irradiation, such as the alloying effect (c-loop densities are less numerous in M5™ than in RXA Zy-4) or the preferential c-loop nucleation around some precipitates. Furthermore, thanks to the hydrogen atoms penetration depth, proton irradiations allow to obtain a bulk material fully irradiated and to avoid the free surface effect. This therefore appears as a good tool to study the role of hydrogen on c-loops.

On the other hand, Zr ion irradiations performed at 573 K, also induce c-loops in the material, but the microstructure is not representative of the neutron irradiated material. However, Zr ion irradiation appears to be a good tool to study the effect of stress on c-loops, one of the reasons being the low power deposited by the ion beam.

The differences observed between the two types of irradiations are well explained by the differences in damage rates. Thus, Zr ion irradiations would probably be more representative of neutron irradiations by using a higher irradiation temperature.

The effect of stress on c-loops has been studied for the first time. These results first show that a stress applied at the beginning of the irradiation has no impact on the c-loop microstructures. On the contrary, an effect is observed when a stress is applied when c-loops are already created. This phenomenon is well explained by the SIPA mechanism which describes the effect of stress on irradiation microstructures.

Then, the effect of pre-hydriding on c-loops has been studied for the first time. A strong effect of the pre-hydriding is observed. In the matrix, far from precipitated hydrides, the c-loop density is higher and the microstructure more homogeneous in the pre-hydrided material than in the control samples. Moreover, c-loop "bundles" are observed in the alignment of what seem to be former hydrides partially or completely dissolved.

These results can be explained by the fact that hydrogen could influence c-loop microstructures by two different mechanisms:
- On the one hand, the growth of the c-loop nuclei could be enhanced by the trapping of hydrogen atoms in solid solution on the defects, reducing the loop energy. In this mechanism, the precipitated hydrides act as source of hydrogen atoms.
- On the other hand, the remaining <c+a> dislocations after the precipitated hydrides dissolution could act as nucleation sites for c-loops.

Due to the low hydride density the role of c-loop bundles created on former hydrides is believed to remain minor. On the other hand, the increase of c-loop density within all the grains of the material can have a significant consequence on the accelerated growth of recrystallized zirconium alloys.

These experimental results prove that an applied stress can have an effect on c-loops. Furthermore, these results also show that pre-hydriding leads to an increase of the c-loop densities after proton irradiations. Since c-loops are responsible for the growth acceleration of recrystallized Zr alloys, these two effects could have a significant impact on the in-reactor deformation of the fuel assemblies.

7. References

1. Franklin, D.G., G. Lucas, and A. Bement, *Creep of Zirconium Alloys in Nuclear Reactors*. Vol. STP 815. 1983: ASTM. 284.
2. Franklin, D.G. and R.B. Adamson, *Implications of Zircaloy Creep and Growth to Light Water-Reactor Performance*. Journal of Nuclear Materials, 1988. **159**: p. 12-21.
3. Onimus, F. and J.-L. Bechade, *Radiation Effects in Zirconium Alloys*, in *Comprehensive Nuclear Materials*, R. Konings, Editor 2012, Elsevier Ltd. Oxford. p. 1-31.
4. Carpenter, G.J.C., R.H. Zee, and A. Rogerson, *Irradiation Growth of Zirconium Single-Crystals - A Review*. Journal of Nuclear Materials, 1988. **159**: p. 86-100.
5. Lemaignan, C. and A.T. Motta, *Zirconium Alloys in Nuclear Applications*, in *Materials Science and Technology*, VCH, Editor 1994. p. 455.
6. Griffiths, M., R.W. Gilbert, and V. Fidleris, *Accelerated Irradiation Growth of Zirconium Alloys*. Zirconium in the Nuclear Industry: Eighth International Symposium, 1989. **STP 1023**: p. 658-677.
7. McGrath, M.A., S. Yagnik, and H. Jenssen, *Effects of Pre-Irradiation on Irradiation Growth & Creep of Re-Crystallized Zircaloy-4*, in *Zirconium in the Nuclear Industry: 16th international symposium* 2010, ASTM: Chengdu, China.
8. Zbib, A., et al. *Recent Channel Bow Events and AREVA's Integrated Solution*. in *2011 Water Reactor Fuel Performance Meeting*. 2011. Chengdu.
9. Holt, R.A. and R.W. Gilbert, *c-Component Dislocations In Annealed Zircaloy Irradiated At About 570-K*. Journal Of Nuclear Materials, 1986. **137**(3): p. 185-189.
10. Jostsons, A., P.M. Kelly, and R.G. Blake, *Nature of Dislocation Loops in Neutron-Irradiated Zirconium*. Journal of Nuclear Materials, 1977. **66**(3): p. 236-256.
11. Griffiths, M., *A Review of Microstructure Evolution in Zirconium Alloys During Irradiation*. Journal of Nuclear Materials, 1988. **159**: p. 190-218.
12. Griffiths, M., M.H. Loretto, and R.E. Smallman, *Anisotropic Distribution of Dislocation Loops in Hvem-Irradiated Zr*. Philosophical Magazine, 1984. **49**(5): p. 613-624.
13. Griffiths, M., et al., *Study of Point-Defect Mobilities in Zirconium During Electron-Irradiation in A High-Voltage Electron-Microscope*. Journal of Nuclear Materials, 1994. **208**(3): p. 324-334.
14. De Carlan, Y., et al., *Influence of Iron in the nucleation of <c> Component Disclocation Loops in Irradiated Zircaloy-4*. Zirconium in the nuclear Industry: Eleventh International Symposium, 1996. **STP 1295**: p. 638-653.
15. Tournadre, L., et al., *Experimental study of the nucleation and growth of c-component loops under charged particle irradiations of recrystallized Zircaloy-4*. Journal of Nuclear Materials, 2012. **425**(1-3): p. 76-82.
16. Yamada, S. and T. Kameyama, *Observation of c-component dislocation structures formed in pure Zr and Zr-base alloy by self-ion accelerator irradiation*. Journal of Nuclear Materials, 2012 **422**(1-3): p. 167-172.
17. Hengstler-Eger, R.-M., et al., *Heavy ion irradiation induced dislocation loops in AREVA's M5 alloy*. Journal of Nuclear Materials, 2012. **423**(1-3): p. 170-182.
18. Foll, H. and M. Wilkens, Phys. Stat. Sol. A, 1977. **39**: p. 561–571.
19. Griffiths, M. and R.W. Gilbert, *The Formation of C-Component Defects in Zirconium Alloys During Neutron-Irradiation*. Journal of Nuclear Materials, 1987. **150**(2): p. 169-181.
20. Griffiths, M., M.H. Loretto, and R.E. Sallmann, Journal Of Nuclear Materials, 1983. **115**(2–3): p. 313–322.
21. De Diego, N., Y.N. Osetsky, and D.J. Bacon, Journal Of Nuclear Materials, 2008. **374**(1–2): p. 87–94.
22. Hull, D. and D.J. Bacon, *Introduction to dislocations*. Vol. 37. 1984: Pergamon Press.
23. A., B., F. A., and A. S., *Transmission electron microscopy studies of dislocations and stacking faults in a hexagonal metal: Zinc*. Acta Metallurgica, 1961. **9**(5): p. 464–490.
24. Hirth, J.P. and J. Lothe, *Theory of Dislocations* 1982., New York: John Wiley and sons.
25. Domain, C., *Simulations atomiques ab initio des effets de l'hydrogène et de l'iode dans le zirconium*, 2002, Université des sciences et technologies de Lille: Lille.
26. Gilbon, D. and C. Simonot, *Effect of Irradiation on the Microstructure of Zircaloy-4*. Zirconium in the Nuclear Industry, Tenth International Symposium, 1994. **STP 1245**: p. 521-548.
27. Christien, F. and A. Barbu, Journal Of Nuclear Materials, 2009. **393**: p. 153–161.
28. Woo, C.H., Journal Of Nuclear Materials, 1988. **159**: p. 237–256.
29. Adamson, R.B., R.P. Tucker, and V. Fidleris, *High-Temperature Irradiation Growth in Zircaloy*. Zirconium in the Nuclear Industry, fifth conference, 1982. **STP 754**: p. 208-234.
30. Griffiths, M., *Microstructure Evolution in Zr Alloys during Irradiation: Dose, Dose Rate, and Impurity Dependence*. Zirconium in the Nuclear Industry: fifteenth International Symposium, 2009. **STP 1505**: p. 19-26.

31. Garner, F.A., W.G. Wolfer, and H.R. Brager, *A Reassessment of the Role of Stress in Development of Radiation-Induced Microstructure.* Effects of Radiation on Structural Materials, 1979. **STP 683**: p. 160-183.

32. Garner, F.A. and D.S. Gelles, *Irradiation creep mechanisms: an experimental perspective.* Journal Of Nuclear Materials, 1988. **159**: p. 286-309.

33. Wolfer, W.G., *Correlation of Radiation Creep Theory with Experimental Evidence.* Journal Of Nuclear Materials, 1980. **90**(1-3): p. 175-192.

34. Leteurtre. J, J.L. Pouchou, and Zuppiroli. L, *Experimental Method For Determining Dislocation Loop Nucleus Size.* Philosophical Magazine, 1973. **27**(6): p. 1323-1334.

35. Matthews, J.R. and M.W. Finnis, *Irradiation Creep Models - An Overview.* Journal Of Nuclear Materials, 1988. **159**: p. 257-285.

36. Brager, H.R., F.A. Garner, and G.L. Guthrie, *Effect of Stress on Microstructure of Neutron-Irradiated Type-316 Stainless-Steel.* Journal Of Nuclear Materials, 1977. **66**(3): p. 301-321.

37. Wolfer, W.G. and M. Ashkin, *Stress-Induced Diffusion of Point-Defects to Spherical Sinks.* Journal of Applied Physics, 1975. **46**(2): p. 547-557.

38. Heald, P.T. and M.V. Speight, *Point-Defect Behavior in Irradiated Materials.* Acta Metallurgica, 1975. **23**(11): p. 1389-1399.

39. Hellouin de Menibus, A., et al., *Hydrogen contribution to the thermal expansion of hydrided Zircaloy-4 cladding tubes.* Journal of Nuclear Materials, 2013. **440**(1-3): p. 169-177.

40. Bossis, P., et al., *In PWR Comprehensive Study of High Burn-Up Corrosion and Growth Behavior of M5^R and Recrystallized Low-Tin Zircaloy-4.* Zirconium in the Nuclear Industry, fifteenth International Symposium, 2009. **STP 1505**: p. 430-456

41. McMinn, A., E.C. Darby, and J.S. Schofield, *The Terminal Solid Solubility of Hydrogen in Zirconium Alloys.* Zirconium in the nuclear industry: twelfth international symposium, 2000. **STP 1354**: p. 173-195.

42. Vizcaino, P., A.D. Banchik, and J.P. Abriata, *Solubility of hydrogen in Zircaloy-4: irradiation induced increase and thermal recovery.* Journal of Nuclear Materials, 2002. **304**(2-3): p. 96-106.

43. Lewis, M.B., *Deuterium-Defect Trapping in Ion-Irradiated Zirconium.* Journal of Nuclear Materials, 1984. **125**(2): p. 152-159.

44. Vizcaino, P., A.D. Banchik, and J.P. Abriata, *Hydrogen in Zircaloy-4: effects of the neutron irradiation on the hydride formation.* Journal of Materials Science, 2007. **42**(16): p. 6633-6637.

45. Chung, H.M., et al., *Characteristics of Hydride Precipitation and Reorientation in Spent-Fuel Cladding.* Zirconium in the nuclear industry: thirteenth international symposium, 2002. **STP 1423**: p. 561 - 582.

46. Tournadre, L., et al., *Toward a better understanding of the hydrogen impact on the radiation induced growth of zirconium alloys.* Journal of Nuclear Materials, 2013. **441**(1-3): p. 222-231.

47. Mardon, J.-P., D. Charquet, and J. Senevat, *Influence of Composition and Fabrication Process on Out-Of-Pile and In-Pile Porperties of M5 Alloy.* ASTM, 2000. **STP 1354**: p. 505-524.

48. Damcott, D.L., et al., *A radiation effects facility using a 1.7 MV tandem accelerator.* Nuclear Instruments and Methods in Physics Research Section B, 1995. **99**(1–4): p. 780–783.

49. Zu, X.T., et al., *Effect of proton and Ne irradiation on the microstructure of Zircaloy 4.* Philosophical Magazine A-Physics of Condensed Matter Structure Defects and Mechanical Properties, 2005. **85**(4-7): p. 649-659.

50. Kearns, J.J., *Diffusion-Coefficient of Hydrogen in Alpha Zirconium, Zircaloy-2 and Zircaloy-4.* Journal Of Nuclear Materials, 1972. **43**(3): p. 330-&.

51. Bernas, H., et al., *Progress report on Aramis, the 2 MV tandem at Orsay.* Nuclear Instruments and Methods in Physics Research, Section B, 1992. **623**(3): p. 416–420.

52. Cottereau, E., et al., *ARAMIS: An ambidextrous 2 MV accelerator for IBA and MeV implantation.* Nuclear Instruments and Methods in Physics Research Section B, 1990. **45**(1–4): p. 293–295.

53. Ruault, M.-O., et al., *In situ Transmission Electron Microscopy Ion Irradiation Studies at Orsay.* Journal of Materials Research, 2005. **20**(7): p. 1758-1768.

54. Carassou, S., et al., *REFLET Experiment in OSIRIS: Relaxation under Flux as a Method for Determining Creep Behavior of Zircaloy Assembly Components.* Journal of ASTM International, 2010. **7**(8).

55. Shishov, V.N., et al., *Influence of Neutron irradiation and Dislocation Structure and Phase Composition of Zr-Base Alloys.* Zirconium in the Nuclear Industry: Seventh International Symposium, 1987. **STP 939**: p. 603-622.

56. Tournadre, L., et al., *Experimental study of the nucleation and growth of c-component loops under charged particle irradiations of recrystallized Zircaloy-4.* Journal Of Nuclear Materials, Corrected proof, doi: 10.1016/j.jnucmat.2011.11.061(0).

57. Sawatzky, A., *Hydrogen in Zircaloy-2: its distribution and heat of transport.* Journal Of Nuclear Materials, 1960. **2**(4): p. 321-328.

58. Christien, F. and A. Barbu, *Effect of self-interstitial diffusion anisotropy in electron-irradiated zirconium: A cluster dynamics modeling.* Journal Of Nuclear Materials, 2005. **346**(2-3): p. 272-281.

59. Was, G.S., *Fundamentals of Radiation Materials Science*2007, Berlin Heidelberg: Springer-Verlag.

60. Etienne, A., et al., *Tomographic atom probe characterization of the microstructure of a cold worked 316 austenitic stainless steel after neutron irradiation.* Journal Of Nuclear Materials, 2008. **382** p. 64–69.
61. Meslin, E., et al., *Characterization of neutron-irradiated ferritic model alloys and a RPV steel from combined APT, SANS, TEM and PAS analyses.* Journal Of Nuclear Materials, 2010. **406**: p. 73–83.
62. Ribis, J., et al., *Experimental study and numerical modelling of the irradiation damage recovery in zirconium alloys.* Journal Of Nuclear Materials. **403**(1-3): p. 135-146.
63. Kearns, J.-J., *Dissolution kinetics of hydride platelets in zircaloy-4.* Journal of Nuclear Materials, 1968. **27**(1): p. 64.
64. Domain, C. and A. Legris, *Investigation of glide properties in hexagonal titanium and zirconium: An ab initio atomic scale study*, in *Iutam Symposium on Mesoscopic Dynamics of Fracture Process and Materials Strength,* 2004, Springer: Dordrecht. p. 411-420.
65. Girardin, G. and D. Delafosse, *Solute-dislocation interactions: modelling and experiments in hydrogenated nickel and nickel base alloys.* Materials Science and Engineering A, 2004. **387-389**: p. 51-54.
66. Oudriss, A., et al., *The diffusion and trapping of hydrogen along the grain boundaries in polycrystalline nickel.* Scripta Materialia, 2012. **66**: p. 66-40.
67. Puls, M.P., *The Effect of Hydrogen and Hydrides on the Integrity of Zirconium Alloy Components*, Springer-Verlag: London.
68. Shinohara, Y., et al., *In Situ TEM Observation of Growth Process of Zirconium Hydride in Zircaloy-4 during Hydrogen Ion Implantation.* Journal of Science and Technology, 2009. **46**(6): p. 564-571.
69. Griffiths, M., et al., *HVEM study of the effects of alloying elements and impurities on radiation damage in Zr-alloys.* Journal Of Nuclear Materials, 1993. **205**: p. 273-283.
70. Yoo, M.H. and C.T. Wei, *Application of Anisotropic Elasticity Theory to the Plastic Deformation in Hexagonal Zinc.* Philosophical Magazine, 1966. **13**: p. 759-775.
71. Yoo, M.H., *c+a dislocation reactions in H.C.P. metals.* Scripta Metallurgica, 1968. **2**: p. 537-540.